2014

Glutamate transporter modulation of ambient and synaptic glutamate levels

Weinan Sun

GLUTAMATE TRANSPORTER MODULATION OF AMBIENT AND SYNAPTIC GLUTAMATE LEVELS

By

Weinan Sun

BS in Biotechnology, China Pharmaceutical University, Jiangsu, China, 2008

Dissertation

presented in partial fulfillment of the requirements
for the degree of

Doctor of Philosophy
in Neuroscience

The University of Montana
Missoula, MT

Spring 2014

Approved by:
Sandy Ross, Dean of The Graduate School
Graduate School

Dr. Michael P. Kavanaugh, Chair
Department of Biomedical and Pharmaceutical Sciences

Dr. Richard J. Bridges
Department of Biomedical and Pharmaceutical Sciences

Dr. J. Joshua Lawrence
Department of Biomedical and Pharmaceutical Sciences

Dr. Nicholas R. Natale
Department of Biomedical and Pharmaceutical Sciences

Dr. Sarah J. Certel
Division of Biological Sciences

Dr. Leonid V. Kalachev
Department of Mathematical Science

ProQuest LLC.
789 East Eisenhower Parkway
P.O. Box 1346
Ann Arbor, MI 48106 - 1346

Sun, Weinan, Ph.D, January 2014 Major

Neuroscience

GLUTAMATE TRANSPORTER MODULATION OF AMBIENT AND SYNAPTIC GLUTAMATE LEVELS

Chairperson: Michael P. Kavanaugh, Ph.D.

Abstract

Glutamate is the major excitatory neurotransmitter in the mammalian central nervous system. An accurate spatial and temporal glutamate concentration profile during signaling is crucial for reliable neural computation. In these studies, we investigated the roles of glutamate transporters in controlling both ambient glutamate levels and dynamic glutamate concentrations profiles during synaptic transmission. Using the Xenopus oocyte expression system, we demonstrated that glutamate transporters act as an effective sink and are capable of maintaining >200 fold glutamate concentration gradient between the bath and cell surface when expressed at levels corresponding to physiological transporter densities in the CNS. We also characterized the specificity and actions of a new arylasparate glutamate transport inhibitor at the Shaffer collateral-CA1 pyramidal cell synapse in hippocampus, and demonstrated that glial glutamate transporters tightly control synaptically released glutamate and further, through cooperation with voltage-dependent Mg^{2+} block, they influence the magnitude and frequency-dependence of postsynaptic NMDA receptor signaling.

ACKNOWLEDGMENTS

Upon the completion of my Ph.D study, I would like to thank many individuals for their continuous support, inspiration and friendship: my committee- Dr. Richard Bridges, Dr. Josh Lawrence, Dr. Nicholas Natale, Dr. Sarah Certel and Dr. Leonid Kalachev; my friends and coworkers- Katie Hoffmann, Alicia Angell, Greg Leary, Sarj Patel, Vaishali Satpute, Loretta Bolyard, Shailesh Agarwal, David Holley, David Bonislawski, Jordan Pauli, Avi Rascoe, Jenny Lind, Feng Yi, Tarun Gupta, Juan Palacios, Jonathan Andrews. I want to give a special thank you to my Ph.D advisor Dr. Mike Kavanaugh who patiently guided me through failures and showed me how to do rigorous and significant science and co-worker Greg Leary who inspired me with his selfless personality, work ethics and kindness to everyone around him. I want to thank my mother Jingfeng Xie and my father Fuxin Sun for their unconditioned love and support. I am glad to have shared the journey with all these amazing people and ready to further my passion on studying the brain in my future science endeavors.

Table of Contents

LIST OF FIGURES

CHAPTER 1 : BACKGROUND AND SIGNIFICANCE

Glutamate transporter subtypes and expression density.

Glutamate is considered to be the major excitatory neurotransmitter involved in most aspects of normal brain functions including neural development, cognition, learning and memory. (Danbolt, 2001). Due to the importance of glutamate in excitatory signaling, its actions need to be tightly regulated. Elevated glutamate levels under neurological diseases such as stroke and epilepsy can cause significant activation of NMDA receptors and Ca^{2+} entry, which lead to excitotoxicity and eventually cell death. Unlike acetylcholine which is enzymatically degraded after release, glutamate must be actively taken up intracellularly by glutamate transporters. Five major subtypes of glutamate transporters exist in the CNS, EAAT1-5. EAAT1 (GLAST) and EAAT2 (GLT-1) are the only glutamate transporters expressed in brain astrocytes, EAAT3 (EAAC1) and EAAT4 are predominately neuronal, whereas EAAT5 is preferentially expressed in the retina (Lehre and Danbolt, 1998; Danbolt, 2001). EAAT1 and EAAT2 are densely expressed in both hippocampus and cerebellum, with the numbers of EAAT1 and EAAT2 3200 and 12,000 per μm^3 in the stratum radiatum of adult rat hippocampus and 18,000 and 2800 in the cerebellar molecular layer, respectively (Lehre and Danbolt ,1998). Glutamate transporters expressed near a single release site greatly out number the glutamate molecules released by a synaptic vesicle (~3000 molecules per vesicle).

Tissue concentrations of glutamate transporters

	mg/gm tissue	μM	Molecules per μm^3	Membrane $\mu m^2/\mu m^3$	Molecules per μm^2
Stratum radiatum, hippocampus CA1					
GLAST	0.32	5.3	3200	1.4	2300
GLT	1.3	20	12000	1.4	8500
Stratum moleculare, cerebellum					
GLAST	1.8	29	18000	3.8	4700
GLT	0.30	4.7	2800	3.8	740
EAAT4[b]	0.2	3.2	1900	1.1	1800

Table 1.1, Summary of transporter surface and volumetric density of GLAST and GLT-1 in CA1 hippocampus and molecular layer of cerebellum (Lehre and Danbolt , 1998).

Biophysical and structural properties of glutamate transporters.

The glutamate transporter belongs to the class of secondary-active, sodium dependent transporters, which transport glutamate utilizing pre-existing ion gradients between the extracellular solution and cytoplasm. The stoichiometry of glutamate transport coupling is movement of 1 glutamate$^-$, 3 Na^+ and 1 proton into the cell along with 1 K^+ out of the cell (Zerangue and Kavanaugh, 1996), since 2 net charges are moved into the cell with each transporter cycle, this process is electrogenic (Figure 1.1).

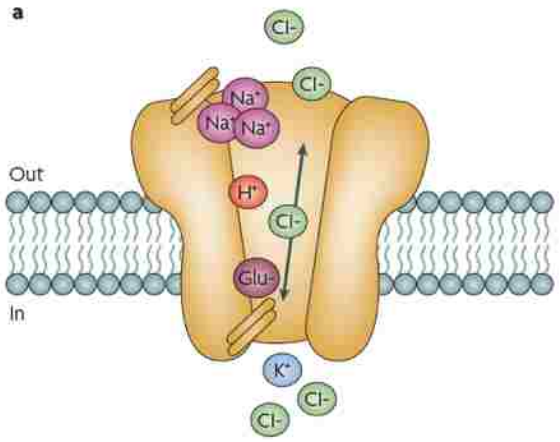

Figure 1.1. Stoichiometry of glutamate transport. Schematic of a glutamate transporter with coupled (Na^+, K^+, and H^+) and uncoupled (Cl^-) ions. (Tzingounis and Wadiche, 2007)

In addition to coupled ions, glutamate transporters also behave as glutamate gated Cl^- channels, and upon transport of glutamate, an anion current also pass through the transporter. Both of the coupled current and uncoupled anion current can be recorded when expressing glutamate transporter in either Xenopus oocyte system (Wadiche et al., 1995) or HEK cell line (Bergles et al., 2002). When puffing glutamate onto outside out patches pulled from EAAT2 expressing HEK cells with different intracellular solutions, kinetics comparison can be made between the coupled and uncoupled currents. Transporter associated anion currents has been shown to exhibit rise and decay time twice as slow as the coupled currents (Figure 1.2, Bergles et al., 2002).

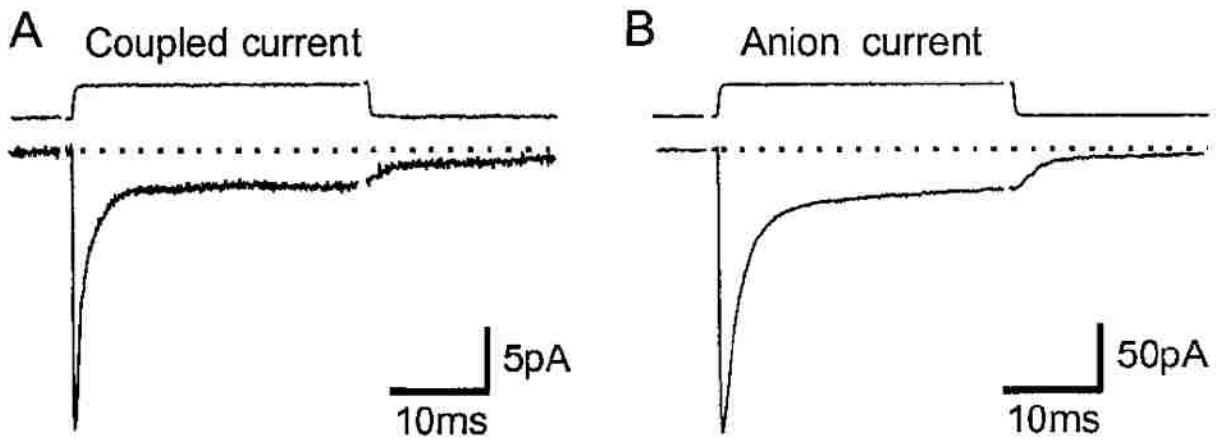

Figure 1.2. Comparison of coupled and uncoupled responses elicited by L-glutamate. A) L-Glutamate-evoked (10mM) transporter current from an outside-out patch recorded in the absence of permeant anions (K-gluconate-based internal solution.) B) L-Glutamate-evoked (10mM) transporter current from an outside-out patch recorded in the presence of permeant anions (KSCN-based internal solution.) (Bergles et al., 2002)

Currents recorded during these electrogenic processes are important indexes reflecting protein conformation changes associated with glutamate binding and transport. Transporter currents measured from recombinantly or natively expressed glutamate transporters have provided us some important knowledge of the transporter kinetics. Binding of glutamate to the transporters has been shown to be very rapid, on the order of $10^7 M^{-1}s^{-1}$ (Otis and Jahr, 1998; Wadiche and Kavanaugh, 1998; Grewer et al., 2000), similar to the binding rate of glutamate to AMPARs and NMDARs; glutamate translocation can be as rapid as 1-3ms in GLT-1 (Otis and Kavanaugh, 2000). The rate limiting step of glutamate transport has been purposed to be the transport turnover rate: at physiological potentials (-80mV to -90mV) the turnover rate of EAAT2 was estimated to be $100s^{-1}$ (Bergles and Jahr, 1998; Bergles et al., 2002) which is around 1.5 times and 6 times faster than the turnover rates for EAAT3 and EAAT1 (Grewer et al., 2000; Wadiche and Kavanaugh, 1998). These slow turnover rate estimates raised the questions that how transporters regulate the spatiotemporal profile of the glutamate concentration profile in the synaptic cleft on the time scale of a few milliseconds when the turnover rate is so slow (~10ms -

60ms). One hypothesis suggests that instead of removing glutamate molecules by glutamate translocation, glutamate transporters effectively reduce glutamate concentration mainly by ligand binding (Tong and Jahr, 1994). With 15200 glutamate transporters per μm^3 in hippocampal neuropil (Lehre and Danbolt, 1998), 3000 molecules released from a single vesicle can be effectively removed from the extracellular space by binding within 100μs. Besides glutamate transporters' fast binding rate and high density, a low capture efficiency also makes them an ideal buffer for g lutamate. Capturing efficiency is defined as the probability of a glutamate molecules bound to a glutamate transporter will be transported into the cytosol rather than be unbound back into the extracellular space. Capturing efficiency for EAAT1-3 has been determined by kinetic modeling to be approximately 0.5 (Wadiche and kavanaugh, 1998; Bergles et al., 2002; Tzingounis, 2002) . This suggests that a bound glutamate molecule is likely to unbind from one transporter and release back to the extracellular space and encounter other transporters until being transported. Low capturing efficiency helps effectively localizing the glutamate signal by spreading glutamate sequestering tasks among a focal region instead of overwhelm the transporters in immediate region of release. Different translocation rate of the subtypes of glutamate transporter can further fine tune the system by mixing "buffers" (low capture efficiency) with "transporters" (high capture efficiency) and be effective at modulating both fast and slow glutamate signals (buffer and transport are contrasted in Figure 1.3). In the hippocampus, EAAT1 and EAAT2 may function as different roles according to their kinetics. Due to EAAT2 faster transport rate (Bergles et al., 2002) , it may work mainly as sinks to keep low ambient glutamate levels, whereas EAAT1 works as buffers and play an more important role during synaptic transmission.

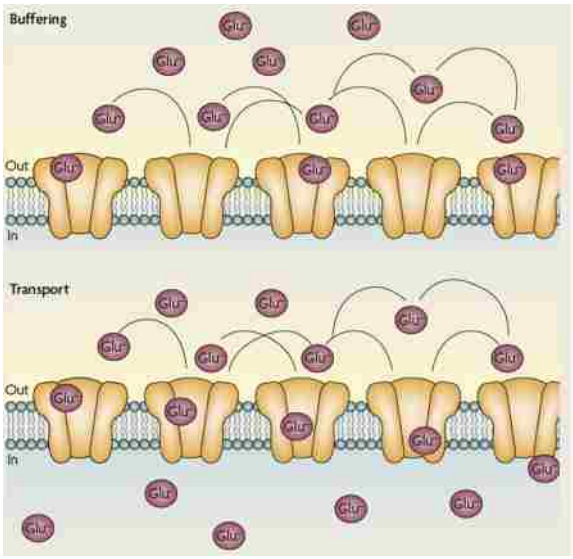

Figure 1.3. Comparison of buffer mode and transport mode of glutamate transporters. In buffer mode, a bound glutamate molecule is more like to unbind than being transported. On the contrary, in transport mode, a bound glutamate molecule is more likely to be transported than to unbind. (Tzingounis and Wadiche, 2007)

The crystal structure of a bacterial glutamate transporter homologue was solved by Yernool et al. in 2004 and provided new insights on mechanisms of glutamate transport. This structure shows that glutamate transporters are homomers composed of three identical subunits which form a significant bowl shape structure that extends halfway across the membrane bilayer (Figure 1.4). This central cavity within glutamate homotrimer protein has been proposed to reduce the energy for transport (Gouaux and MacKinnon 2005) and restrict ligand diffusion (Leary et al., 2011). Leary et al. demonstrated that the unbinding rate of an EAAT3 ligand 2-FAA was 9 times faster when co-applied with saturating concentration of glutamate than the unbinding rate when no glutamate was applied; this suggests the central cavity restrict glutamate unbinding from the protein. Effects of the bowl would further increase the complexity of the transporter kinetics, since ligand unbinding rate is no longer constant with varying [Glu] but changing with the occupancy of transporter subunits.

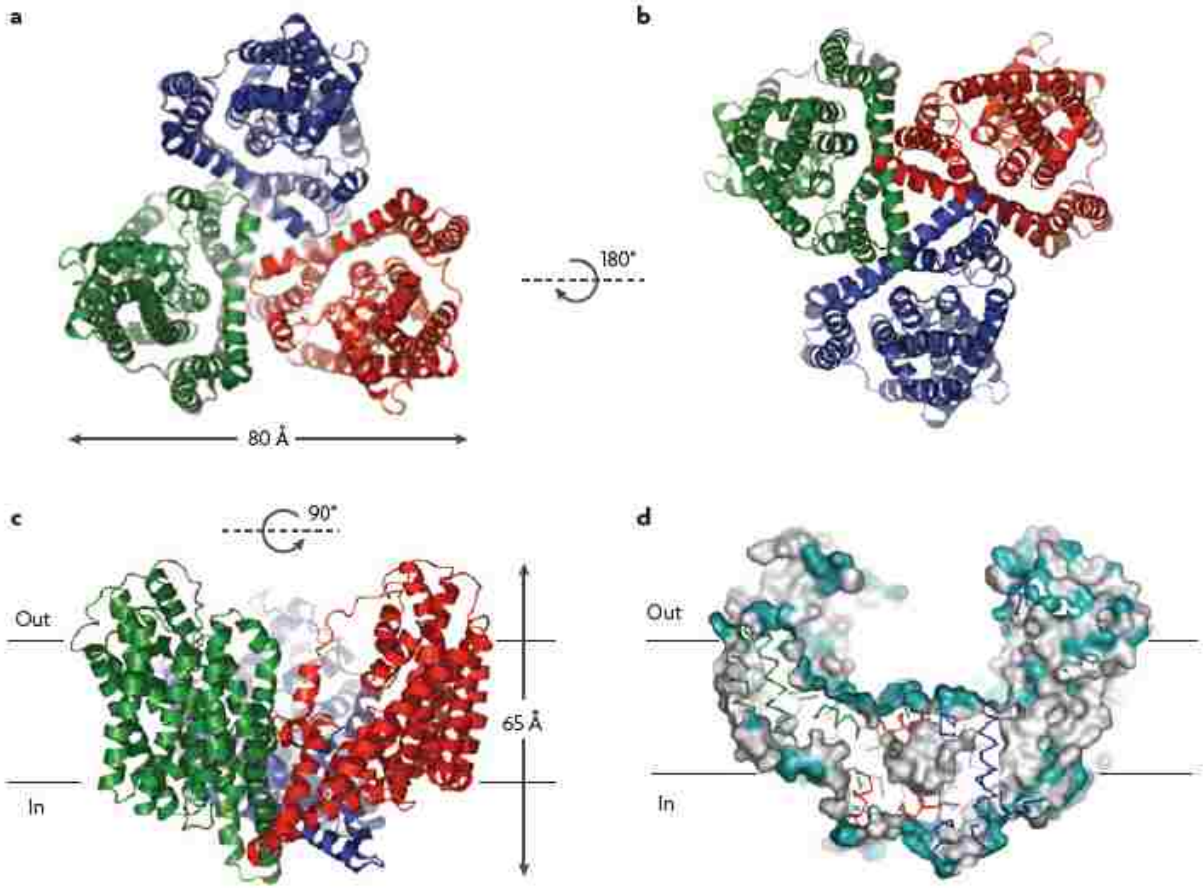

Figure 1.4. The crystal structure of a bacterial glutamate transporter. a) A ribbon representation of Glt_{ph}, viewed from the extracellular side of the membrane. b) A view of the trimer from the cytoplasm. c) A view of the trimer from the plane of the membrane. d) A surface representation of the trimer sliced through the center. Polar and non-polar residues are colored cyan and white. (Yernool et al., 2004; Tzingounis and Wadiche, 2007)

Ambient glutamate levels and tonic glutamate release in the brain.

Based on the thermodynamic coupling of glutamate transporter, an extracellular [Glu] as low as 2nM can be maintained in the absence of glutamate release (Zerangue and Kavanaugh, 1996; Levy et al. 1998). However, tonic activation of NMDAR by ambient glutamate has been observed (Sah et al. 1989; Cavelier and Attwell, 2005; Herman and Jahr, 2007), and ambient glutamate level in the hippocampus was estimated to be on the order of 25nM. In addition, microdialysis measurements in vivo reported extracellular [Glu] on the order of 2μM (Benveniste et al., 1984; Lerma et al., 1986; for reviews see Cavelier et al., 2005, Nyatrai et al., 2006). This suggests a constant release of glutamate is present in vivo and this constant release is

considered to be of glial origin (Jabaudon et al. 1999, Cavalier et al., 2005). An accurate estimation of ambient [Glu] is important since ambient [Glu] levels significantly influence the extent of activation and desensitization of glutamate receptors (Figure 1.5).

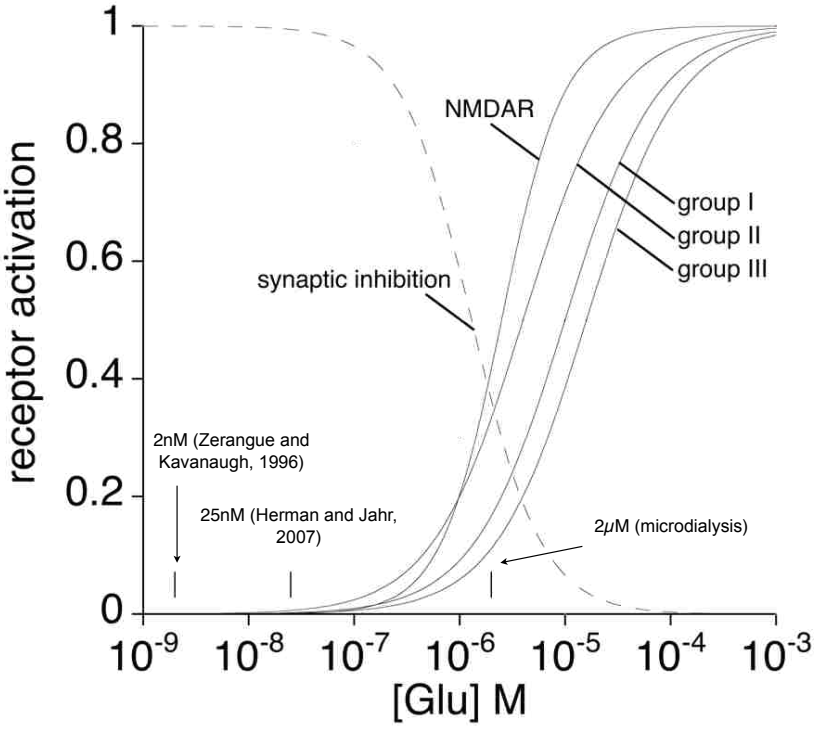

Figure 1.5. Glutamate concentration-dependance of ionotropic and metabotropic receptor activation. NMDAR data (logistic fit, n=1.5) from Patneau and Mayer, 1990. Representative high affinity members of group I-III metabotropic receptor affinities from Pin and Duvoisin, 1995. Dashed line shows glutamate concentration-dependance of inhibition of synaptic NMDAR signaling in cultured neurons, reflecting pre- and post-synaptic mechansisms (Zorumski et al., 1996).

Glutamate transporter's roles on synaptic transmission.

In addition to glutamate transporter's role on keeping low tonic glutamate levels, they also help to shape phasic glutamate signal during synaptic transmission. The effects of glutamate transporters on synaptic signals differ from one synapse to another, as examples, the hippocampal CA3-CA1 synapse and cerebellar Purkinje cell synapses will be discussed.

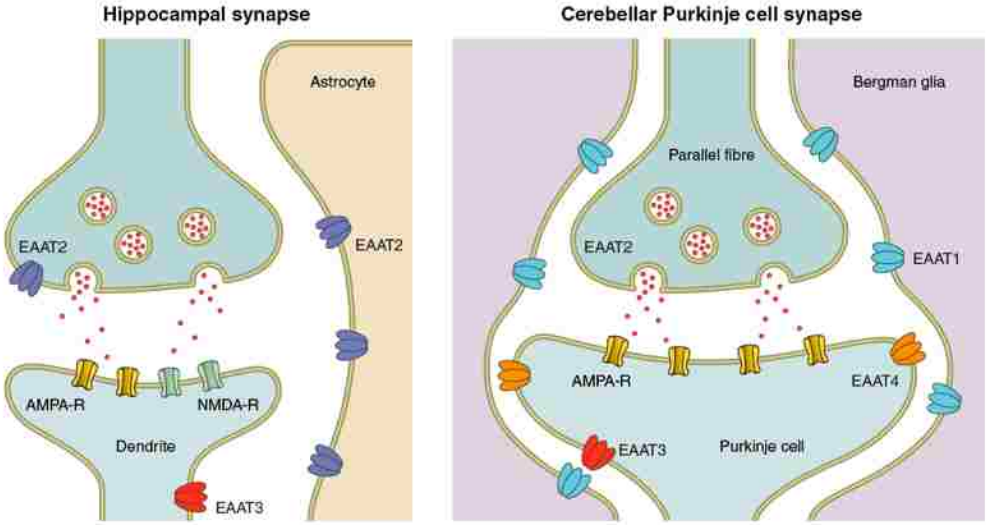

Figure. 1.6. Schematic diagrams of the glutamatergic CA1 hippocampal synapse and the cerebellar Purkinje cell synapse showing the predominat pre- and postsynaptic locations and glial cell locations of the EAAT subtypes. (Vandenberg and Ryan, 2013)

Hippocampal CA3-CA1 synapse

Earlier studies using substrate inhibitors such as L-trans-PDC concluded that both AMPAR and NMDAR post-synaptic responses are not regulated by glutamate transporters and diffusion is the major mechanism for fast glutamate clearance (Hestrin et al., 1990; Sarantis et al., 1993; Isaacson and Nicoll, 1993). With the development of non-substrate transporter blockers such as TBOA (Shimamoto et al., 1998), TFB-TBOA (Shimamoto et al., 2004) and L-TBA (Esslinger et al., 2005), the roles of glutamate transporter on AMPAR and NMDAR responses were revealed. And currently, the consensus for glutamate transporter's role in synaptic transmission is that glutamate uptake does not acutely shape AMPAR responses but significantly limits NMDAR activation (Tzingounis and Wadiche, 2007); When recorded in 0 Mg^{2+}

or depolarized potentials (eg. +40mV) transporters block by these non-substrate inhibitors caused a significant prolongation of NMDAR EPSCs, in contrast, AMPAR EPSC kinetics are not significantly altered except when desensitization is blocked (Tsukada et al., 2005). However, glutamate transporter's roles under physiological conditions (non-voltage clamp, with physiological Mg^{2+}) are less well characterized. The aim of chapter 3 and 4 of this dissertation is to betters understand how transporters modulate NMDAR and AMPAR responses under physiological conditions.

Cerebellar synapses

In contrast to CA3-CA1 synapses which are only marginally covered by glial processes (less than 50%, Ventura and Harris, 1999), the cerebellar Bergmann glial cells closely appose Purkinje cell synapses (Spacek, 1985, Figure 1.6). This unique spatial arrangement of glial processes not only provide a physical barrier between neighboring synapses, but also bring transporters closer to release sites; this also support the fact that transporter blockers have more robust effects on cerebellar synaptic transmission than that is seen in the hippocampus. Transporter blockers have significantly different effects on two of the major cerebellar synapses: parallel fiber synapses and climbing fiber synapses. At parallel fiber synapses, transporter block has little effect on AMPAR EPSCs following single/sparse axonal stimulation, the effects gets bigger when stimulating multiple adjacent axons (Barbour et al., 1994). In contrast, glutamate transporters limit the time course of AMPAR activation following a single synaptic stimulation (Wadiche and Jahr, 2001). In addition to glial transporter EAAT1 and EAAT2, neuronal transporter EAAT4 also plays an important role in controlling cerebellar synaptic transmission. Evidences have suggest that EAAT4 limits extrasynaptic receptor activation by buffering synaptically released glutamate (Tsai et al., 2012).

In summary, glutamate transporters with different kinetics long with specific extracellular morphologies cooperatively shape the profile of synaptically released glutamate.

References

Barbour B, Keller BU, Llano I, Marty A. (1994) Prolonged presence of glutamate during excitatory synaptic transmission to cerebellar Purkinje cells. Neuron. 12(6):1331-43.

Benveniste H, Drejer J, Schousboe A, Diemer NH. (1984) Elevation of the extracellular concentrations of glutamate and aspartate in rat hippocampus during transient cerebral ischemia monitored by intracerebral microdialysis. J Neurochem. 43(5):1369-74.

Benveniste H, Drejer J, Schousboe A, Diemer NH. (1987) Regional cerebral glucose phosphorylation and blood flow after insertion of a microdialysis fiber through the dorsal hippocampus in the rat. J Neurochem. 49(3):729-34

Bergles DE, Tzingounis AV, Jahr CE. (2002) Comparison of coupled and uncoupled currents during glutamate uptake by GLT-1 transporters. J Neurosci. 22(23):10153-62.

Cavelier P, Attwell D (2005) Tonic release of glutamate by a DIDS-sensitive mechanism in rat hippocampal slices.564(Pt 2):397-410.

Cavelier P, Hamann M, Rossi D, Mobbs P, Attwell D. (2005) Tonic excitation and inhibition of neurons: ambient transmitter sources and computational consequences. Prog Biophys Mol Biol.87(1):3-16.

Clapp-Lilly KL, Roberts RC, Duffy LK, Irons KP, Hu Y, Drew KL. (1999) An ultrastructural analysis of tissue surrounding a microdialysis probe. J Neurosci Methods. 90(2):129-42.

Danbolt NC (2001) Glutamate uptake. Prog Neurobiol. 65(1):1-105.

Esslinger CS, Agarwal S, Gerdes J, Wilson PA, Davis ES, Awes AN, O'Brien E, Mavencamp T, Koch HP, Poulsen DJ, Rhoderick JF, Chamberlin AR, Kavanaugh MP, Bridges RJ. (2005) The substituted aspartate analogue L-beta-threo-benzyl-aspartate preferentially inhibits the neuronal excitatory amino acid transporter EAAT3. Neuropharmacology.49(6):850-61.

Furuta A, Rothstein JD, Martin LJ (1997) Glutamate transporter protein subtypes are expressed differentially during rat CNS development. J. Neurosci 17:8363-8375

Gouaux E, Mackinnon R. (2005) Principles of selective ion transport in channels and pumps. Science. 310(5753):1461-5.

Grewer C, Watzke N, Wiessner M, Rauen T. (2000) Glutamate translocation of the neuronal glutamate transporter EAAC1 occurs within milliseconds. Proc Natl Acad Sci U S A.97(17): 9706-11.

Herman MA, Jahr CE. (2007) Extracellular glutamate concentration in hippocampal slice. J Neurosci. 27(36):9736-41.

Hestrin S, Sah P, Nicoll RA. (1990) Mechanisms generating the time course of dual component excitatory synaptic currents recorded in hippocampal slices.Neuron. 5(3):247-53.

Jabaudon D, Shimamoto K, Yasuda-Kamatani Y, Scanziani M, Gähwiler BH, Gerber U (1999) Inhibition of uptake unmasks rapid extracellular turnover of glutamate of nonvesicular origin. Proc. Natl. Acad. Sci. U.S.A 96:8733-8738.

Lehre KP, Danbolt NC. (1998) The number of glutamate transporter subtype molecules at glutamatergic synapses: chemical and stereological quantification in young adult rat brain. J Neurosci.18(21):8751-7.

Le Meur K, Galante M, Angulo MC, Audinat E. (2007) Tonic activation of NMDA receptors by ambient glutamate of non-synaptic origin in the rat hippocampus. J Physiol.580 (Pt. 2):373-83.

Leary GP, Holley DC, Stone EF, Lyda BR, Kalachev LV, Kavanaugh MP. (2011) The central cavity in trimeric glutamate transporters restricts ligand diffusion. Proc Natl Acad Sci U S A. 108(36):14980-5.

Lerma J, Herranz AS, Herreras O, Abraira V, Martín del Río R. (1986) In vivo determination of extracellular concentration of amino acids in the rat hippocampus. A method based on brain dialysis and computerized analysis. Brain Res. 384(1):145-55.

Nyitrai G, Kékesi KA, Juhász G. Extracellular level of GABA and Glu: in vivo microdialysis-HPLC measurements. (2006) Curr Top Med Chem. 6(10):935-40.

Rossi DJ, Oshima T, Attwell D. (2000) Glutamate release in severe brain ischaemia is mainly by reversed uptake. Nature. 403(6767):316-21.

Otis TS, Jahr CE. (1998) Anion currents and predicted glutamate flux through a neuronal glutamate transporter. J Neurosci.18(18):7099-110.

Otis TS, Kavanaugh MP. (2000) Isolation of current components and partial reaction cycles in the glial glutamate transporter EAAT2. J Neurosci. 20(8):2749-57.

Sah P, Hestrin S, Nicoll RA. (1989) Tonic activation of NMDA receptors by ambient glutamate enhances excitability of neurons. Science. 246(4931):815-8.

Sarantis M, Ballerini L, Miller B, Silver RA, Edwards M, Attwell D. (1993) Glutamate uptake from the synaptic cleft does not shape the decay of the non-NMDA component of the synaptic current. Neuron. 11(3):541-9.

Shimamoto K, Lebrun B, Yasuda-Kamatani Y, Sakaitani M, Shigeri Y, Yumoto N, Nakajima T. (1998) DL-threo-beta-benzyloxyaspartate, a potent blocker of excitatory amino acid transporters. Mol Pharmacol. 53(2):195-201.

Shimamoto K, Sakai R, Takaoka K, Yumoto N, Nakajima T, Amara SG, Shigeri Y. (2004) Characterization of novel L-threo-beta-benzyloxyaspartate derivatives, potent blockers of the glutamate transporters. Mol Pharmacol. 65(4):1008-15.

Spacek J. (1985) Three-dimensional analysis of dendritic spines. III. Glial sheath. Anat Embryol (Berl).171(2):245-52.

Supplisson S, Bergman C. (1997) Control of NMDA receptor activation by a glycine transporter co-expressed in Xenopus oocytes. J Neurosci. 17(12):4580-90.

Tong G, Jahr CE. (1994) Block of glutamate transporters potentiates postsynaptic excitation. Neuron.13(5):1195-203.

Tsai MC, Tanaka K, Overstreet-Wadiche L, Wadiche JI. (2012) Neuronal glutamate transporters regulate glial excitatory transmission. J Neurosci. 32(5):1528-35.

Tzingounis, A. and Wadiche, J. Nature Reviews Neuroscience (2007) Glutamate transporters: confining runaway excitation by shaping synaptic transmission. 8(12):935-47.

Vandenberg, R.J., Ryan, R.M., 2013. Mechanisms of glutamate transport. Physiol. Rev. 93, 1621–1657.

Ventura R, Harris KM. (1999) Three-dimensional relationships between hippocampal synapses and astrocytes. J Neurosci. ;19(16):6897-906.

Wadiche, J.I., Arriza, J.L., Amara, S.G., and Kavanaugh, M.P. (1995). Kinetics of a human glutamate transporter. Neuron 14, 1019–1027.

Wadiche JI, Kavanaugh MP. (1998) Macroscopic and microscopic properties of a cloned glutamate transporter/chloride channel. J Neurosci. 18(19):7650-61.

CHAPTER 2: GLUTAMATE TRANSPORTER CONTROL OF AMBIENT GLUTAMATE LEVELS

Weinan Sun, Denis Shchepakin, Leonid V. Kalachev and Michael P. Kavanaugh

Abstract

Accurate knowledge of the ambient extracellular glutamate concentration in brain is required for an understanding of its potential impact on tonic and phasic receptor signaling. Estimates of ambient glutamate based on microdialysis measurements are generally in the range of ~2-7 μM, approximately 100-fold higher than estimates based on electrophysiological measurements of tonic NMDA receptor activity (25-90 nM). The latter estimates are closer to the estimated thermodynamic limit of glutamate transporters (2 nM). The reasons for this discrepancy are not known, but it has been suggested that microdialysis measurements could overestimate ambient extracellular glutamate because of reduced glutamate transporter activity in a region of metabolically impaired neuropil adjacent to the dialysis probe. We explored this issue by measuring diffusion gradients created by varying densities of glutamate transporters expressed in *Xenopus* oocytes. With free diffusion from a fixed 10 μM glutamate source, the surface concentration of glutamate depended on transporter density and was reduced over 2 orders of magnitude by transporters expressed at membrane density levels similar to those reported in hippocampus. We created a diffusion model to simulate the effect of transport impairment on microdialysis measurements with boundary conditions corresponding to a 100 μm radius probe. A gradient of metabolic disruption in a thin (~100 μm) region of neuropil adjacent to the probe increased predicted [Glu] in the dialysate over 100-fold. The results provide support for electrophysiological estimates of submicromolar ambient extracellular [Glu] in brain and provide a possible explanation for the higher values reported using microdialysis approaches.

Introduction

During synaptic transmission, glutamate transporters restrict the spatiotemporal pattern of ionotropic and metabotropic glutamate receptor signaling (for review see Tzingounis and Wadiche, 2007). In addition to their roles in shaping the dynamics of synaptically released glutamate, glutamate transporters also help maintain low steady-state glutamate levels. Given the stoichiometry of ion coupling to glutamate uptake, the theoretical lower limit of extracellular glutamate in brain is approximately 2 nM (Zerangue and Kavanaugh, 1996; Levy et al., 1998). Many studies using intracerebral microdialysis have reported levels of ambient glutamate ≥ 2 μM, three orders of magnitude higher than the theoretical lower limit (Benveniste et al., 1984; Lerma et al., 1986; for reviews see Cavelier et al., 2005, Nyatrai et al., 2006). By contrast, reports of ambient glutamate concentration estimated from electrophysiological measurement of tonic NMDA receptor activity in hippocampal slice range from 25 to 89 nM (Cavelier and Attwell, 2005; Le Meur et al., 2007; Herman and Jahr, 2007).

Accurate knowledge of the ambient glutamate concentration in different brain regions is important for evaluating its effects on synaptic transmission. Several ionotropic and metabotropic glutamate receptor subtypes are activated by low micromolar concentrations of glutamate, and tonic exposure in this range profoundly inhibits synaptic circuitry *in vitro* (Zorumski et al., 1996). Glutamate transporters play a dominant role in limiting ambient glutamate (Danbolt, 2001; Tzingounis and Wadiche, 2007). Pharmacological inhibition of transport has been shown to lead to a rapid increase in glutamate from largely non-vesicular sources, causing increased tonic NMDA receptor signaling (Jabaudon et al., 1999; Cavelier and Attwell, 2005; Le Meur et al., 2007, Herman and Jahr, 2007).

In this work we attempt to review and integrate data in the literature with new *in vitro* measurements and *in vivo* modeling of diffusion gradients formed by glutamate transporters. Proceeding from the assumption that in steady-state conditions, the volume-averaged rates of release and uptake of glutamate are equal, we demonstrate the strong influence of glutamate transporter membrane density on steady-state diffusion gradients and suggest that metabolic

impairment of glutamate transport in a shallow boundary region of a microdialysis probe can account for the discrepancies between estimates of ambient glutamate from dialysis and electrophysiological approaches.

Materials and methods

Xenopus oocyte recording

Approximately 50ng of human EAAT3 cRNA was microinjected into stage V-VI Xenopus oocytes and recordings were made 1-6 d later. Recording solution contained 96mM NaCl, 2mM KCl, 1mM $MgCl_2$, 1.8mM $CaCl_2$, and 5mM Hepes (pH 7.5). Microelectrodes were pulled to resistances between 1 and 3MΩ and filled with 3M KCl. Data were recorded with Molecular Devices amplifiers and analog-digital converters interfaced to Macintosh computers. Data were analyzed offline with Axograph X (v.1.0.8) and KaleidaGraph (v 3.6; Synergy) software. For stopped flow measurements, oocytes were voltage clamped at -60 mV in a perspex recording chamber in which glutamate depletion in the absence of perfusion was <1% of the total in the recording chamber**.** Transporter surface density was estimated from current measurements assuming a coupled current of 2 charges/cycle at E_{Cl} (-20 mV), turnover rate of 15/sec, oocyte surface area 2.85×10^7 μm^2, and transport voltage-dependance of e-fold/76 mV (Wadiche et al., 1995; Zerangue and Kavanaugh, 1996).

Mathematical modeling of [Glu] profile near the microdialysis probe

Our microdialysis probe model can be described by diffusion equation in polar coordinates with sink and leak in right hand sides:

$$\partial u/\partial t = D \cdot (1/r) \cdot \partial/\partial r \, [r \cdot \partial u/\partial r] - J \cdot u/(K_m + u) + K_L$$

where u corresponds to glutamate concentration. The first term in the right hand side is a Laplace operator in polar coordinates multiplied by a diffusion coefficient D. The second term represents the Michaelis-Menten transporter sink in the tissue, and the third term K_L represents the leak, which is constant in damaged and healthy tissue. The parameter J is a function of distance from the probe center r, which describes the transporters spatial impairment between the healthy and damaged tissue. Because the spatial metabolic damage is approximated as a Gaussian curve, we define the function J as

$J(r) = 0$ when $0 \leq r \leq L$

$J(r) = J_{max} \cdot \{1-e^{[-(r-L)^2/2 \cdot sigma^2]}\}$ when $r > L$

where L is the radial boundary for the microdialysis probe and sigma represents the distance from the probe boundary characterizing the Gaussian damage function. The boundary conditions for the model are:

$\partial u/\partial r|_{r=0} = 0$

$u(t,\infty) = u_s$

The initial condition is

$u(t,r) = u^*$ when $0 \leq r \leq L$

$u(t,r) = u_s$ when $r > L$

This model cannot be solved analytically because of the nonlinear term in the right hand side of equation, so it was solved numerically by space discretization, which transforms it into system of ordinary differential equations.

Estimation of volumetrically averaged glutamate leak in hippocampus

The leak rate constant (K_L) was estimated by assuming ambient [Glu] = 25nM (Herman and Jahr 2007), a glutamate transporter concentration of 140μM (140-250μM, Lehre and Danbolt 1998), a transporter K_M = 25μM, and a maximal transporter turnover rate J_{max} = 25 molecules/ sec

The leak was then calculated by the equation below:

$K_L = u_{ambient}/(K_m + u_{ambient}) \cdot [GluT] \cdot J_{max} = 2100$ molecules x μm^{-3} x sec^{-1}

where [GluT] is the volumetric concentration of glutamate transporters.

Results

Diffusive concentration gradients formed by glutamate transporters

Co-expression studies of NMDA receptors with transporters for its co-agonists glycine and glutamate have shown that transporters can limit receptor activity by establishing diffusion-limited transmitter concentration gradients (Supplisson and Bergman, 1997; Zuo and Fang, 2005). We studied the concentration gradients formed by passive diffusion from an quasi-infinite glutamate source in a perspex chamber to the glutamate sink established by transporters on the cell surface (see methods). Oocytes expressing the human neuronal glutamate transporter EAAT3 were voltage-clamped at -60 mV and superfused with varying concentrations of glutamate at a linear flow rate of 20 mm/sec flow followed by a stopped-flow interval (Figure 2.1). Steady-state currents elicited by glutamate perfusion relaxed to a lower steady-state level when flow was stopped, and following resumption of flow, currents rapidly recovered to initial values. The reduction in current amplitude during zero flow conditions was likely due to the formation of a diffusion-limited concentration gradient resulting in reduced surface [Glu], because the ratio of the current amplitudes with and without flow were dependent on the

concentration of glutamate in the perfusate (Figure 2.1 B,C and D). This was also manifested as a significant shift in the K_M value for glutamate measured by the concentration-dependance of steady-state currents in flow and stopped-flow conditions (32 ± 2 μM and 216 ± 37.0 μM, respectively, n=4; p=0.0014), while the I_{max} values were not significantly different.

Figure 1

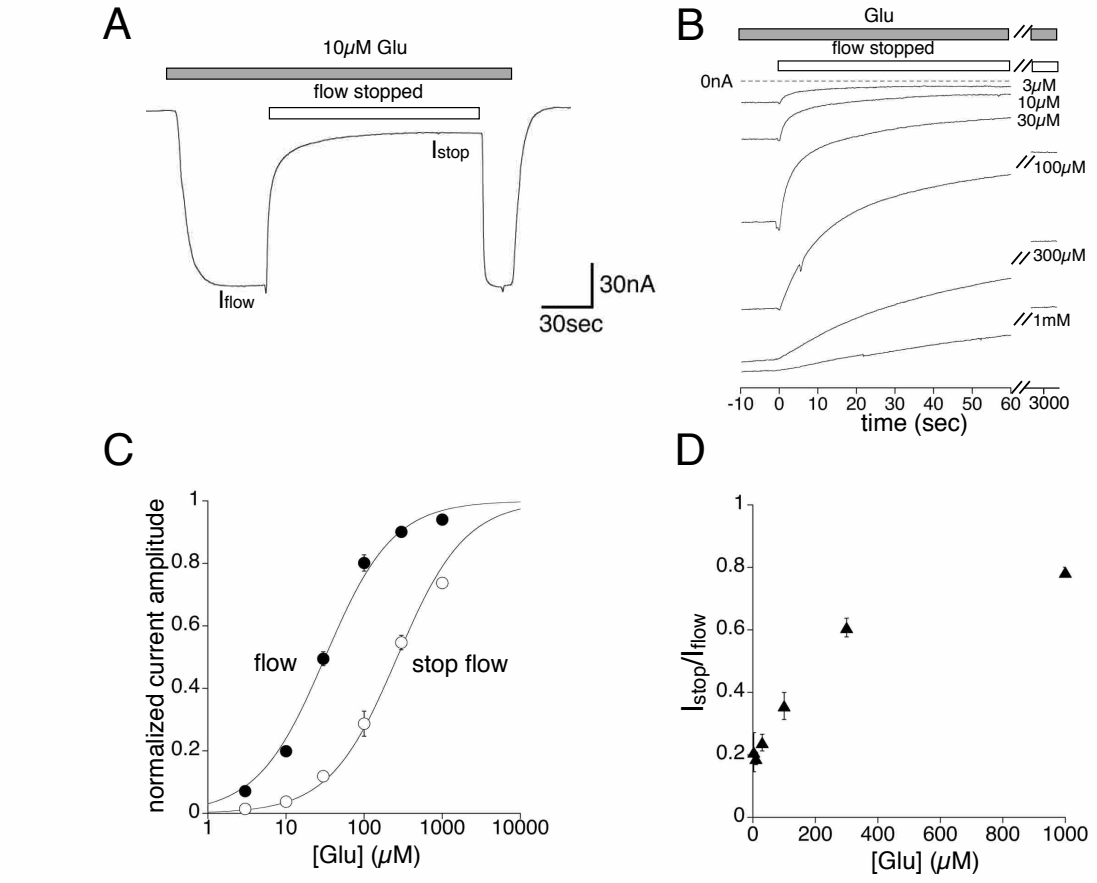

Figure 2.1: Glutamate transport acts as a sink to form a concentration gradient between the extracellular volume and the membrane surface. A) Current induced by 10μM glutamate decays to a lower steady state flow under stopped-flow conditions at -60mV. B) Current responses to varying [Glu] with and without flow at -60mV. C) Glutamate concentration-dependance of steady-state currents in flow and stopped- flow conditions. (Km value with flow: 32 ± 2 μM; stopped-flow: 215 ± 37 μM; n=4, p=0.0014)

Transporter density effects on surface [Glu]

Glutamate transporters are expressed at different densities among structures in the CNS, and transporter density and/or kinetics can be altered in different pathological

circumstances such as trauma and ischemia. Because steady state ambient [Glu] reflects a homeostatic balance of uptake and leak sources, changes in transport may result in significantly different steady state glutamate levels. We tested the influence of the surface density of glutamate transporters on the concentration gradient formed by passive glutamate diffusion during stopped-flow experiments by monitoring currents induced by 10 μM glutamate. With increasing transporter expression levels, the steepness of the concentration gradient formed during stopped-flow conditions was also increased, as reflected in the changing ratio of the steady-state currents (Figure 2.2A,B).

Even with a fast flow rate, oocyte membranes have a microvillar structure that can act as tortuous diffusion barrier (see Supplisson and Bergman, 1997), and evidence for formation of a concentration gradient between the cell surface and bulk solution was observed. In a group of 29 oocytes with varying expression levels, steady-state K_M values measured with chamber flow (20mm/sec) increased approximately 4-fold as transporter current induced by 1mM glutamate increased from ~200 to ~1100 nA (Figure 2C,D). In order to accurately estimate the concentration of glutamate at the cell surface in stopped flow conditions by comparison of steady state currents with and without flow, it is necessary to correct for the effect of the concentration gradient that transporters establish even with high flow rates, which will cause an overestimation of the K_M value. We fit a linear function relating the measured K_M value to the transport current density (Barry and Diamond 1984; r=0.78; Figure 2D). Extrapolation of this line yielded an estimate of the intrinsic K_M value of approximately 27 μM as transporter density approaches zero.

Figure 2

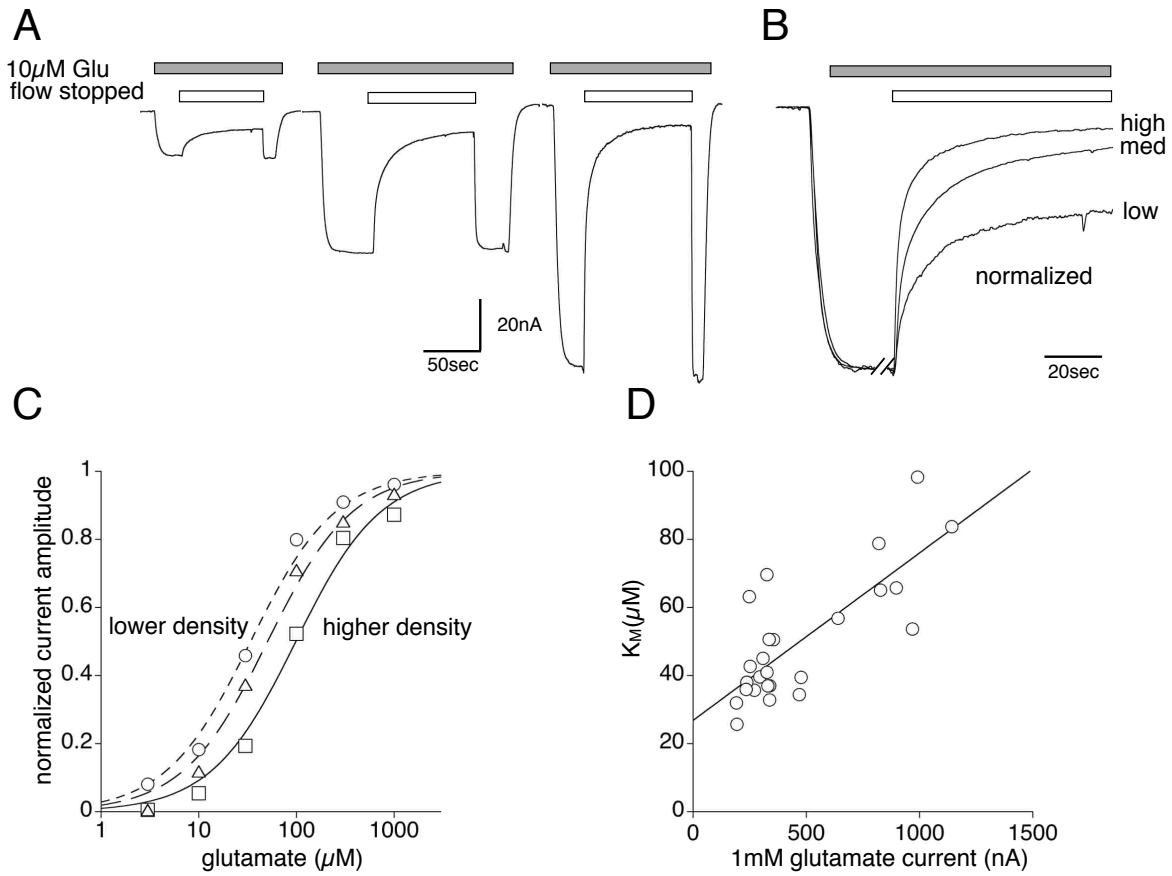

Figure 2.2: Glutamate concentration gradients are a function of transporter density. A) Representative traces of stopped-flow experiments with oocytes expressing different transporter densities. B) Currents from cells in (A) normalized to the steady state current. C) Glutamate concentration-dependance of steady-state currents with low, medium and high expression levels. (Km values: low expression: 33μM , medium expression: 50μM and high expression: 98μM. Transport current amplitudes (1 mM glutamate) are 260nA, 332nA and 688nA respectively). D), K_M values from 29 oocytes with different expression levels (fitted with linear regression, r = 0.78; y intercept = 26.8μM).

Surface [Glu] as a function of transporter density.

The dependance of steady-state K_M on transporter density reflects the fact that the true glutamate concentration at the cell surface is reduced by uptake. However, the concentration difference associated with the diffusion gradient is smaller with higher applied concentrations of glutamate. In 29 oocytes, we recorded currents induced by 1 mM glutamate perfusion to define a Michaelis-Menten function for each cell, and then recorded steady-state current amplitudes in response to 10 μM glutamate in the chamber under stopped-flow conditions. By finding the glutamate concentration corresponding to each current amplitude from the Michaelis-Menten function, we estimated the actual glutamate surface concentration in the stopped-flow condition for each cell (Figure 2.3A and inset). As transporter density increased, the normalized 10μM glutamate amplitude diverged further from the Michaelis-Menten function, suggesting that as the magnitude of the sink increased, the actual surface glutamate concentration diverged further below 10μM. The estimated surface concentration was then plotted as a function of transporter density (see methods), which revealed a supralinear effect of transporter density on surface [Glu] (Figure 3B). Transporter density in this group of cells ranged from 234 to 5165 transporters per μm^2. At low expression levels, the estimated [Glu] approached the chamber concentration (10 μM). At transporter densities of ~5000 μm^{-2} (approaching estimates in hippocampus of 10800 μm^{-2}; Lehre and Danbolt 1998), surface [Glu] was estimated to be 54 nM, roughly 185-fold lower than [Glu] in the chamber.

Figure 3

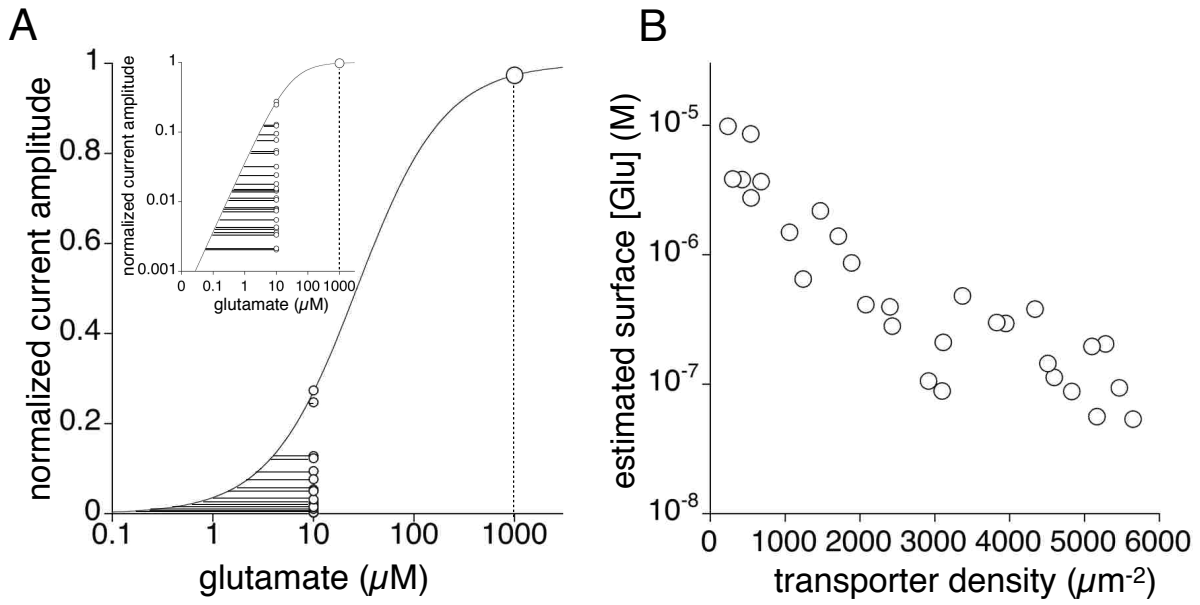

Figure 2.3: Surface [Glu] estimates as a function of transporter density.

Surface [Glu] estimated from relative amplitude of steady state current amplitude without flow to the 1mM steady state glutamate current with flow fitted to Michaelis-Menten function (K_M=26.8 μM) (A, semi-log plot; inset, double-log plot) and plotted as a function of transporter density (B) for each oocyte at -60mV.

Modeling the glutamate concentration profile near a microdialysis probe

We constructed a diffusion model to simulate the spatial profile of glutamate near a microdialysis probe (see methods). From quantitative immunoblotting, the glutamate transporter density in hippocampus has been estimated to be between 0.14 and 0.25 mM (Lehre and Danbolt, 1998). From the transporter density, glutamate transport averaged over a given volume of neuropil can be estimated for any given ambient glutamate value based on Michaelis-Menten kinetics (neglecting exchange, which becomes significant as ambient glutamate approaches the

equilibrium thermodynamic limit). At steady state, sources and sinks are equal, and the steady-state leak and uptake of glutamate are equal. With ambient [Glu] = 25nM (Herman and Jahr, 2007) and transporter density of 0.14 mM, the volume-averaged steady-state glutamate leak is predicted to be approximately 2100 molecules μm^{-3} sec^{-1} (but see Cavelier and Attwell, 2005). This tonic leak will cause increased ambient glutamate if transport is reduced as could occur in a metabolically impaired region of neuropil near a microdialysis probe (Clapp-Lilly, 1999; Bungay et al., 2003; Benveniste et al., 1987). Using the transporter density estimate from Lehre and Danbolt (1998) and assuming ambient [Glu] = 25 nM (Herman and Jahr 2007), we constructed a model with partial differential equations describing the spatial profile of [Glu] near a 100μm radius microdialysis probe with an adjacent region with a Gaussian gradient of impaired transport (Figure 4A). Although transporter reversal can occur with severely impaired ion gradients, we assume a constant leak in the region of damage, which may underestimate the effect of metabolic damage on glutamate measured in the probe. Starting the simulation at time = 0 with no glutamate in the interior of the probe, the glutamate concentration rises with an exponential time constant ~ 8.5 sec to a steady state level (data not shown). At steady state, [Glu] inside the probe is elevated relative to the healthy region far from the probe (Figure 2.4B_1). With sigma = 0 (i.e. no tissue damage), [Glu] in the probe is equal to the ambient [Glu] in the healthy tissue. With gradients of damage from sigma = 100 to 300 μm, steady-state glutamate levels in the probe range from ~3 to 10 μM (Figure 4B_1). Decreasing the glutamate diffusion coefficient from its value in buffer, which is higher than in brain (Kullmann et al., 1999), increases the predicted steady state [Glu] measured in the probe (Figure 4B_2). Increasing or decreasing the leak rate L (Figure 4B_3) also influences steady state [Glu] predicted in the probe volume.

Figure 4

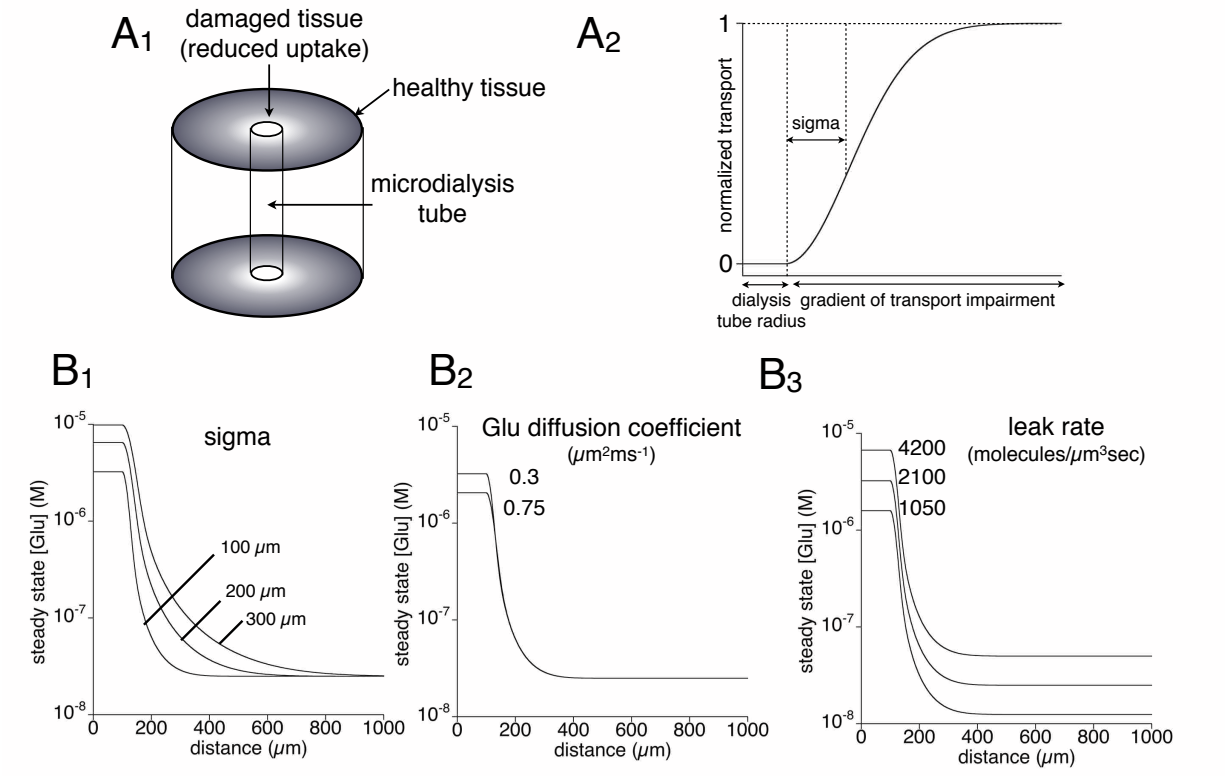

Figure 2.4: Diffusion model of transporter contribution in dialysis measurement. A_1) Cartoon of metabolic damage in Gaussian region surrounding the microdialysis tube. A_2) Reduced uptake rate described by the Gaussian function in the damaged region. B) PDE numerical modeling describing the spatial profile of steady-state [Glu] with varying sigma (B_1), diffusion constant (B_2) and leak rate (B_3).

Discussion

Glutamate transporters limit receptor activity on different time scales in the brain by restricting the spread of synaptically released glutamate as well as by maintaining low ambient glutamate concentrations (for reviews, see Danbolt, 2001; Tzingounis and Wadiche, 2007; Vandenberg and Ryan, 2013). The steady-state ambient concentration of extracellular glutamate at any point in brain reflects the balance of fluxes through sources and sinks in the neuropil. The data presented here indicate that glutamate transporters expressed on cell

membranes establish transporter density-dependent concentration gradients when glutamate is supplied by passive diffusion from an infinite source. Data presented in this work shows that at transporter densities similar to those reported in hippocampal membranes (~$10^4/\mu m^2$; Lehre and Danbolt, 1998) the concentration gradient between a 10 μM bulk medium concentration and the cell surface exceed two orders of magnitude. The steepness of the gradient formed will be further increased if diffusion is reduced by e.g. increased membrane tortuosity (Kullmann et al 1999). Conversely, reduction of transporter density or activity will reduce the steepness of the gradient and increase [Glu] at the cell surface. Reduced glutamate transport by loss or metabolic impairment is implicated in a broad range of neurodegenerative disorders including stroke (Rossi et al., 2000), traumatic brain injury (Goodrich et al., 2013), epilepsy (Coulter and Eid, 2012), Huntington's disease (Faideau et al., 2010), and ALS (Rothstein, 2009).

While a precise knowledge of the concentration of ambient glutamate in various brain regions in normal and neuropathological conditions is clearly desirable, reports of this value in the literature vary widely, with microdialysis approaches consistently providing estimates approximately two orders of magnitude greater than estimates based on electrophysiological measurement of tonic glutamate receptor activity. In the absence of transporter inhibition, ambient [Glu] has been reported as too low to activate AMPA receptors, even when desensitization is pharmacologically blocked (Le Meur et al., 2007). However, ambient [Glu] has been reported to tonically activate high-affinity NMDA receptors (Sah et al., 1989; Cavelier and Attwell, 2005; Le Meur et al., 2007, Herman and Jahr, 2007). Several patch clamp studies in acute hippocampal slice have provided estimates of ambient [Glu] based on analyses of the tonic NMDA receptor currents in CA1 pyramidal neurons. These have been reported as ~25 nM at 32°C (Herman and Jahr, 2007), 27-33 nM at 25°C and 77-89 nM at 35°C (Cavelier and Attwell, 2005), and 83-87 nM at 25°C (Le Meur et al., 2007). These estimates are not likely to be artifactually low due to loss of glutamate from the surface of the slice, because inclusion of 2 μM glutamate in the recording buffer did not alter the level of tonic receptor activity (Herman and Jahr 2007). The major source of glutamate in these studies was of non-vesicular origin. A range

of possible molecular mechanisms may underlie glutamate release, including glutamate-permeable channels, the cystine-glutamate exchanger xCT, and passive membrane diffusion (Kimelberg et al., 1990; Baker et al., 2002; Cavelier and Attwell, 2005; for review see Cavelier et al., 2005). Elevation of ambient [Glu] by inhibition of glutamine synthetase suggests a major contribution of glutamate release from glia (Cavelier and Attwell, 2005, Le Meur et al., 2007).

The data and diffusion model presented here suggests that disrupted glutamate transport could underlie the important quantitative discrepancy between the low ambient glutamate estimates provided by the electrophysiological studies summarized above and those from numerous microdialysis studies which generally report ambient [Glu] values in the range of ~2 μM (reviewed by Cavelier et al., 2005; Featherstone and Shippy, 2008). Histological analyses of tissue surrounding microdialysis probes provide evidence for a layer of damaged tissue surrounding the probe site (Clapp-Lilly, 1999; Bungay et al., 2003; Amina et al., 2003; Jaquins-Gerstl et al., 2009). We propose that disrupted transport in this region could lead to artifactually large concentrations in the probe volume. A critical assumption in our model is that the glutamate leak source is constant in a volume of metabolically damaged tissue where transport is impaired. The precise spatial changes in metabolic activity in a traumatized or ischemic region of tissue are unknown, but the assumption that glutamate release is constant is conservative. For example, glutamate release is increased by reversed glutamate transport due to impaired Na/K gradients during metabolic challenge (Rossi et al., 2000). We have simplified the spatial distribution of transporter impairment by assuming a Gaussian distribution, with sigma values as small as 100 μm leading to significant elevation of predicted probe [Glu] (Figure 2.3).

Electrophysiological studies in slice have shown that blocking glutamate uptake leads to increased ambient [Glu] and activation of AMPA and NMDA receptors (Jabaudon et al., 1999, 2000; Cavelier and Attwell, 2005; Le Meur et al., 2007, Herman and Jahr, 2007). Ischemia-induced reversed transport also leads to large increases in extracellular [Glu] (Rossi et al., 2000). Changes in [Glu] in response to physiological changes including drug exposure,

ischemia, and trauma have also been consistently reported using microdialysis approaches (Benveniste et al., 1984; Hagberg et al., 1985; Baker et al., 2002; Del Arco et al., 2003; Nyitrai et al., 2006). Such baseline changes are also predicted by changes in diffusion gradients surrounding a probe as a consequence of increases in glutamate release (Figure 2.3), suggesting that although the absolute value of extracellular [Glu] concentrations are overestimated in the probe dialysate volume, the changes in baseline probe [Glu] may accurately reflect approximately proportional increases in basal glutamate release.

Steady-state glutamate transport rates are considered to be well-approximated by Michaelis-Menten kinetics, but data presented here show that as transporter density increases, measured K_M values can artifactually increase due to large diffusion gradients. If the ambient glutamate concentration in hippocampus is indeed as low as 25 nM (Herman and Jahr, 2007), then hippocampal transporters would be operating at rates approximately three orders of magnitude below their maximal steady-state capacity. This further highlights the importance of high transporter density, which has been reported in hippocampus to be approximately $10^4/\mu m^2$ on astroglial membranes (Lehre and Danbolt, 1998). High transporter density facilitates maintenance of ambient glutamate concentrations far below K_M values and additionally facilitates their buffering and transport action over the wide dynamic range encompassed by tonic and phasic glutamate signaling.

References

Amina S. Khan, Adrian C. Michael. (2003) Invasive consequences of using micro-electrodes and microdialysis probes in the brain. Trends in Analytical Chemistry 22(8) :503-508.

Arriza, J.L., Fairman, W.A., Wadiche, J.I., Murdoch, G.H., Kavanaugh, M.P., and Amara, S.G. (1994). Functional comparisons of three glutamate transporter subtypes cloned from human motor cortex. J. Neurosci. 14, 5559–5569.

Baker DA, Xi ZX, Shen H, Swanson CJ, Kalivas PW. (2002) The origin and neuronal function of in vivo nonsynaptic glutamate. J Neurosci. 22(20):9134-41.

Barry, P.H., and Diamond, J.M. (1984). Effects of unstirred layers on membrane phenomena. Physiol. Rev. 64, 763–872.

Benveniste H, Drejer J, Schousboe A, Diemer NH. (1984) Elevation of the extracellular concentrations of glutamate and aspartate in rat hippocampus during transient cerebral ischemia monitored by intracerebral microdialysis. J Neurochem. 43(5):1369-74.

Benveniste H, Drejer J, Schousboe A, Diemer NH. (1987) Regional cerebral glucose phosphorylation and blood flow after insertion of a microdialysis fiber through the dorsal hippocampus in the rat. J Neurochem. 49(3):729-34

Bungay PM, Newton-Vinson P, Isele W, Garris PA, Justice JB. (2003) Microdialysis of dopamine interpreted with quantitative model incorporating probe implantation trauma. J Neurochem. 86(4):932-46.

Cavelier P, Attwell D (2005) Tonic release of glutamate by a DIDS-sensitive mechanism in rat hippocampal slices.564(Pt 2):397-410.

Cavelier P, Hamann M, Rossi D, Mobbs P, Attwell D. (2005) Tonic excitation and inhibition of neurons: ambient transmitter sources and computational consequences. Prog Biophys Mol Biol.87(1):3-16.

Clapp-Lilly KL, Roberts RC, Duffy LK, Irons KP, Hu Y, Drew KL. (1999) An ultrastructural analysis of tissue surrounding a microdialysis probe. J Neurosci Methods. 90(2):129-42.

Danbolt NC (2001) Glutamate uptake. Prog Neurobiol. 65(1):1-105.

Del Arco A, Segovia G, Fuxe K, Mora F. (2003) Changes in dialysate concentrations of glutamate and GABA in the brain: an index of volume transmission mediated actions? J Neurochem. Apr;85(1):23-33.

Featherstone DE, Shippy SA. (2008) Regulation of synaptic transmission by ambient extracellular glutamate. Neuroscientist. 14(2):171-81.

Hagberg H, Lehmann A, Sandberg M, Nyström B, Jacobson I, Hamberger A. (1985) Ischemia-induced shift of inhibitory and excitatory amino acids from intra- to extracellular compartments. J Cereb Blood Flow Metab. 5(3):413-9.

Herman MA, Jahr CE. (2007) Extracellular glutamate concentration in hippocampal slice. J Neurosci. 27(36):9736-41.

Jabaudon D, Scanziani M, Gähwiler BH, Gerber U. (2000) Acute decrease in net glutamate uptake during energy deprivation. Proc Natl Acad Sci U S A. 97(10):5610-5.

Jabaudon D, Shimamoto K, Yasuda-Kamatani Y, Scanziani M, Gähwiler BH, Gerber U (1999) Inhibition of uptake unmasks rapid extracellular turnover of glutamate of nonvesicular origin. Proc. Natl. Acad. Sci. U.S.A 96:8733-8738.

Jaquins-Gerstl A, Michael AC. (2009) Comparison of the brain penetration injury associated with microdialysis and voltammetry. J Neurosci Methods. 183(2):127-35.

Kullmann DM, Min MY, Asztély F, Rusakov DA (1999) Extracellular glutamate diffusion determines the occupancy of glutamate receptors at CA1 synapses in the hippocampus. Philos. Trans. R. Soc. Lond., B, Biol. Sci 354:395-402.

Lehre KP, Danbolt NC. (1998) The number of glutamate transporter subtype molecules at glutamatergic synapses: chemical and stereological quantification in young adult rat brain. J Neurosci.18(21):8751-7.

Le Meur K, Galante M, Angulo MC, Audinat E. (2007) Tonic activation of NMDA receptors by ambient glutamate of non-synaptic origin in the rat hippocampus. J Physiol.580 (Pt. 2):373-83.

Lerma J, Herranz AS, Herreras O, Abraira V, Martín del Río R. (1986) In vivo determination of extracellular concentration of amino acids in the rat hippocampus. A method based on brain dialysis and computerized analysis. Brain Res. 384(1):145-55.

Nyitrai G, Kékesi KA, Juhász G. Extracellular level of GABA and Glu: in vivo microdialysis-HPLC measurements. (2006) Curr Top Med Chem. 6(10):935-40.

Rossi DJ, Oshima T, Attwell D. (2000) Glutamate release in severe brain ischaemia is mainly by reversed uptake. Nature. 403(6767):316-21.

Sah P, Hestrin S, Nicoll RA. (1989) Tonic activation of NMDA receptors by ambient glutamate enhances excitability of neurons. Science. 246(4931):815-8.

Supplisson S, Bergman C. (1997) Control of NMDA receptor activation by a glycine transporter co-expressed in Xenopus oocytes. J Neurosci. 17(12):4580-90.

Tzingounis, A. and Wadiche, J. Nature Reviews Neuroscience (2007) Glutamate transporters: confining runaway excitation by shaping synaptic transmission. 8(12):935-47.

Vandenberg, R.J., Ryan, R.M., 2013. Mechanisms of glutamate transport. Physiol. Rev. 93, 1621–1657.

Wadiche, J.I., Arriza, J.L., Amara, S.G., and Kavanaugh, M.P. (1995). Kinetics of a human glutamate transporter. Neuron 14, 1019–1027.

Zuo Z, Fang H. (2005) Glutamate transporter type 3 attenuates the activation of N-methyl-D-aspartate receptors co-expressed in Xenopus oocytes. J Exp Biol. 208(Pt 11):2063-70.

CHAPTER 3: SPECIFICITY AND ACTIONS OF AN ARYLASPARTATE INHIBITOR OF GLUTAMATE TRANSPORT AT THE SCHAFFER COLLATERAL-CA1 PYRAMIDAL CELL SYNAPSE

Weinan Sun*, Katie M. Hoffman*, David C. Holley, and Michael P. Kavanaugh

*these authors contributed equally to this work

Abstract

In this study we characterized the pharmacological selectivity and physiological actions of a new arylaspartate glutamate transporter blocker, L-threo-ß-benzylaspartate (L-TBA). At concentrations up to 100 μM, L-TBA did not act as an AMPA receptor (AMPAR) or NMDA receptor (NMDAR) agonist or antagonist when applied to outside-out patches from mouse hippocampal CA1 pyramidal neurons. L-TBA had no effect on the amplitude of field excitatory postsynaptic potentials (fEPSPs) recorded at the Schaffer collateral-CA1 pyramidal cell synapse. Excitatory postsynaptic currents (EPSCs) in CA1 pyramidal neurons were unaffected by L-TBA in the presence of physiological extracellular Mg^{2+} concentrations, but in Mg^{2+}-free solution, EPSCs were significantly prolonged as a consequence of increased NMDAR activity. Although L-TBA exhibited approximately four-fold selectivity for neuronal EAAT3 over glial EAAT1/EAAT2 transporter subtypes expressed in *Xenopus* oocytes, the L-TBA concentration-dependence of the EPSC charge transfer increase in the absence of Mg^{2+} was the same in hippocampal slices from EAAT3 +/+ and EAAT3 -/- mice, suggesting that TBA effects were primarily due to block of glial transporters. Consistent with this, L-TBA blocked synaptically evoked transporter currents in CA1 astrocytes with a potency similar to its block of heterologously expressed glial transporters. Extracellular recording in the presence of physiological Mg^{2+} revealed that L-TBA prolonged fEPSPs in a frequency-dependent manner by selectively increasing the NMDAR-mediated component of the fEPSP during short bursts of activity. The data indicate that glial glutamate transporters play a dominant role in limiting extrasynaptic transmitter diffusion and binding to NMDARs. Furthermore, NMDAR signaling is

primarily limited by voltage-dependent Mg^{2+} block during low-frequency activity while the relative contribution of transport increases during short bursts of higher frequency signaling.

Introduction

Five major subtypes of excitatory amino acid transporters exist in the CNS, and three of these (EAAT1-3; also known as GLAST, GLT-1, and EAAC1) are expressed in forebrain with distinct distribution patterns on astrocytes (EAAT1 and EAAT2) and neurons (EAAT3) (Furuta et al. 1997). Studies utilizing glutamate uptake inhibitors broadly indicate that the transporters play key roles in glutamate homeostasis, and that they can in some cases shape receptor dynamics during synaptic transmission (Tzingounis & Wadiche 2007). While the synaptic effects of glutamate transport inhibition vary widely in different brain regions, studies at the hippocampal Schaffer collateral-CA1 pyramidal cell (SC-PC) synapse generally indicate that transporter activity does not strongly modify synaptic AMPAR responses [Isaacson & Nicoll, 1993; Sarantis et al. 1993; but see Tong & Jahr,1994; Tsukada et al., 2005]. In contrast, extrasynaptic NMDAR activity is enhanced by glutamate uptake block in this region (Asztely et al., 2007; Lozovaya et al., 1999; Diamond, 2001; Arnth-Jensen et al., 2002; Scimemi et al. 2009).

The relative contributions of the glial EAAT1 and EAAT2 and neuronal EAAT3 subtypes to restricting the spread of synaptically released glutamate from the SC-PC synapse is presently unclear. EAAT2 and EAAT3 are the dominant transporters in forebrain astrocytes and neurons, respectively, while EAAT1 is found on forebrain astrocytes at lower levels (Lehre & Danbolt, 1998). The widely used glutamate uptake blocker DL-TBOA blocks EAAT2 and EAAT3-mediated [^{3}H]L-Glu uptake with IC_{50} values approximately seven-fold lower than for EAAT1 (Shimamoto et al., 2000), and studies utilizing DL-TBOA indicate that it can induce spillover of synaptic glutamate onto NMDARs in hippocampus (Asztely et al., 2007; Lozovaya et al., 1999; Diamond, 2001; Arnth-Jensen et al., 2002; Scimemi et al. 2009). More selective inhibition of the postsynaptic neuronal transporter EAAT3 by intracellular ion substitution during whole cell recording or genetic manipulation also leads to augmentation of NMDAR-mediated EPSCs as

well as changes in synaptic plasticity (Diamond, 2001; Scimemi et al. 2009). In addition to uncertainty surrounding the detailed roles of individual EAAT subtypes in hippocampus, another issue concerns the general role of glutamate transport in restricting NMDAR signaling in the hippocampus under physiological conditions, since this effect has only been reported in conditions permissive for channel activity, i.e. voltage clamp of the postsynaptic neuron at positive potentials or in Mg^{2+}-free ACSF (Asztely et al., 2007; Lozovaya et al., 1999; Diamond, 2001; Arnth-Jensen et al., 2002; Scimemi et al. 2009).

Threo-ß-benzylaspartate (TBA) is a new arylaspartate derivative that is structurally related to TBOA, but with a shorter aryl linkage. In contrast to DL-TBOA, L-TBA displays moderate selectivity for the neuronal EAAT3 subtype over EAAT1 and EAAT2 (Esslinger et al., 2005). In this work we show that L-TBA is highly selective for glutamate transporters over ionotropic glutamate receptors expressed on CA1 pyramidal cells and examined its effects on NMDAR activity during synaptic transmission at the Schaffer-CA1 synapse in wild-type and transgenic mice lacking the neuronal EAAT3 glutamate transporter to gain insights into the respective roles of glial and neuronal transporters. We also compared its actions on postsynaptic signaling using voltage clamp as well as extracellular recording to gain insights into the role of transporters in physiological conditions. The data suggest that glial transporters restrict synaptically released transmitter binding to NMDARs to a significantly greater extent than neuronal transporters. Further, voltage-dependent Mg^{2+} block plays a dominant role in limiting NMDAR signaling during low-frequency activity, while the relative influence of transport increases during short bursts of activity.

Materials and Methods

Drugs

Drugs and chemicals were purchased from Sigma, except CNQX and DL-APV, which were from Tocris. L-TBA was synthesized and purified as described (Esslinger et al. 2005) and a stock solution was dissolved in DMSO at 50mM.

Hippocampal slice preparation and recording

CD1 mice (P15-30) were anesthetized with isofluorane and decapitated in accordance with University of Montana IACUC regulations. The brain was rapidly dissected and placed in ice-cold solution containing (in mM): 80 NaCl, 24 $NaHCO_3$, 25 glucose, 75 sucrose, 2.5 KCl, 1.25 NaH_2PO_4, 0.5 $CaCl_2$, 5 $MgCl_2$, 1 ascorbic acid, 3 Na pyruvate. The solution was saturated with 95% O_2 and 5% CO_2 (pH 7.3). 300μm thick coronal hippocampal slices were cut using a vibratome (VT1200S Leica, Germany), then hemisected and placed in artificial cerebral spinal fluid (ACSF) containing (in mM): 126 NaCl, 2.5 KCl, 1.2 $MgCl_2$, 2.4 $CaCl_2$, 1.2 NaH_2PO_4, 11.4 glucose, and 21.4 $NaHCO_3$ saturated with 95%O_2 and 5% CO_2 (pH 7.3) and maintained at 30°C. Slices were allowed at least 1 hour to recover before being placed in a submersion-type recording chamber perfused at 1.6-2.0 ml/minute with ACSF at 30°C. Slices were visualized on an upright fixed-stage microscope (Olympus BX51WI) equipped with IR-DIC optics. The recording pipettes (3-6MΩ resistance) were filled with internal solution containing (in mM): 110 Cs methanesulfonate, 38 CsCl, 10 HEPES, 10 Na-phosphocreatine, 0.1 EGTA, 0.3 Mg-ATP, 0.3 GTP, 5 QX-314, pH=7.3. Series resistance (typically 15-20 MOhm), was monitored and recording was terminated if a change >20% was observed. Holding potential was -60 to -70 mV. 100μM picrotoxin was added to the ACSF for whole-cell recordings and an incision was made between CA3 and CA1. Extracellular field excitatory post synaptic potentials (fEPSPs) were recorded using glass electrodes filled with ACSF. EPSCs and fEPSPs were induced with 100 μs current pulses between 0.1mA - 0.4mA administered through ACSF-filled stimulating pipettes placed in stratum radiatum. Recordings were made with analog-digital converters and amplifiers from Molecular Devices, and data were acquired at 20kHz and filtered at 5-10 kHz. Data were acquired and analyzed with Axograph software (version 1.1.6). EPSC charge transfer changes and fEPSP prolongation were quantified by integrating the area from the normalized peak of the response until 100 ms after the peak. EPSCs and fEPSPs were elicited with alternating single

and paired stimuli at varying intervals, and the response time-integral of the second response was calculated following subtraction of the first. Data are presented as mean ± S.E. and were evaluated by Student's paired t-test or as noted. Nucleated patches were pulled from the soma of CA1 pyramidal neurons of CD1 mice (P10-20) identified under transmitted IR-DIC optics. Intracellular pipette solution contained (in mM): 60 Cs-methanesulfonate, 38 CsCl, 20 Cs_4BAPTA (4*CsOH+BAPTA), 10 HEPES, 10 Na-phosphocreatine, 4 MgATP, and 0.3 NaGTP, 5 QX-314, pH 7.3 (adjusted by HCl or CsOH). Patch recordings were made at 25° in the presence of 20 μM CNQX. L-glutamate (1 mM) was applied for 50ms or 200ms through a 200 μm diameter double-barreled theta tube attached to a piezoelectric bimorph. Solution exchange kinetics were estimated following patch rupture by measuring junction currents during switches between iso- and hypo-osmotic solutions as displayed above receptor current records.

Results

Computational docking of TBA with glutamate transporters

We constructed an EAAT3 model using published homologous archaeal Glt_{Ph} structures (Boudker et al., 2007, Yernool et al., 2004) and docked aryl-aspartate analogs in order to identify and compare plausible structural interactions. A single Na^+ ion was positioned in the structure according to the structural determination of a Tl^+ ion in the Glt_{Ph}/L-3-Br-TBOA complex (Boudker et al., 2007) and corresponding to electrostatic predictions of Na^+ ion binding sites in EAAT3 (Holley & Kavanaugh, 2009). The EAAT3 residues R447 and D444 interact with the γ-carboxylate and the α-amino group of transported glutamate and determine substrate specificity (Bendahan et al., 2000; Teichman & Kanner, 2007). The computationally docked L-TBA complex suggested corresponding electrostatic interactions between the blocker carboxyl and amino groups with the R447 and D444 residues in EAAT3 (Figure 3.1A). The most energetically favorable L-TBA complexes corresponded to the benzyl group orientation of L-3-Br-TBOA that

was determined in the Glt_{Ph} crystal structure, with interactions between the ring and non-polar residues near the tip of HP2. Interestingly, when computational docking of L-TBOA was performed, an energetically favorable conformation was observed that involved an interaction of R447 with the ether group of the blocker. This alternate orientation positions the benzyl group in an ‘up’ conformation perpendicular to the membrane and parallel to TMD7, and aligns it with non-polar residues in TM7, TM8 and HP2 (Figure 3.1B). Docking energies (Table 1) predict that L-3-Br-TBOA could orient in either conformation while L-TBOA is predicted to predominantly align in the perpendicular, ‘up’ orientation, and L-TBA aligns predominantly in the ‘down’ conformation parallel to the membrane plane.

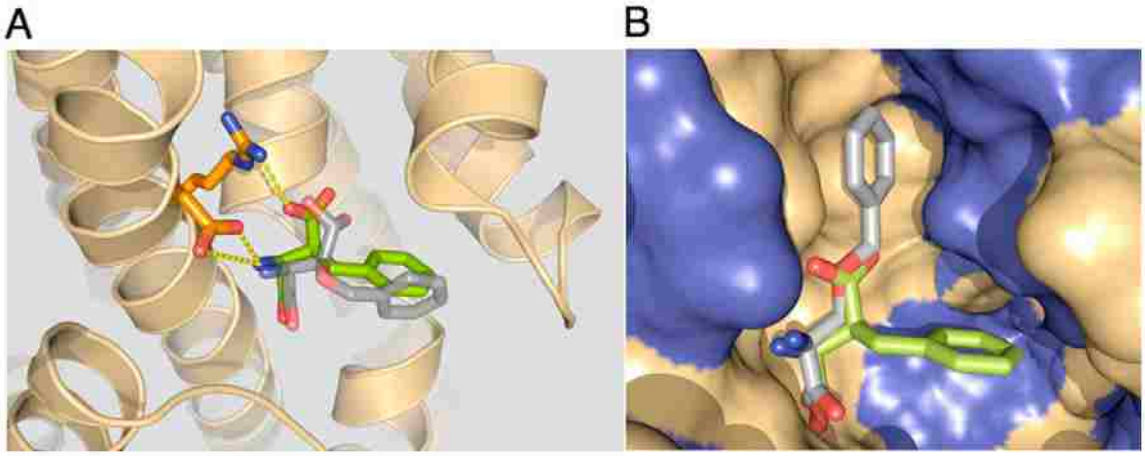

Figure 3.1. Interaction of L-TBA with EAATs. (A) Docking of L-TBA (green) and L-TBOA (gray) in EAAT3 model showing overlap of functional groups interacting with R447 and D444, with benzyl groups oriented toward extracellular loop HP2 as seen in (Esslinger et al., 2005). (B) Surface depiction of the transporter binding site (hydrophobic regions blue) showing L-TBA and alternate docking orientation of L-TBOA with benzyl ring aligned in alternate hydrophobic pocket.

Table 1. Computational docking results.

Structure	ChemScore	ΔG (kJ mol^{-1})	orientation
L-TBOA	18.07	−22.14	perpendicular
L-TBOA	15.01	−18.62	parallel
L-TBA	–	–	perpendicular*
L-TBA	19.70	23.62	parallel
L-3-Br-TBOA	20.19	23.09	perpendicular
L-3-Br-TBOA	18.04	23.90	parallel

*structure not found by energy minimization algorithm.

Interaction of L-TBA with glutamate transporters

L-TBA inhibits uptake mediated by heterologously expressed EAATs, with preference for the neuronal glutamate transporter subtype EAAT3 (Esslinger et al. 2005). However, transport currents mediated by the major glial subtypes are also blocked in *Xenopus* oocytes expressing the transporters (Figure 3.2A,B). To examine the actions of L-TBA on glial transporters in situ, synaptically activated transport currents (STCs) were recorded in astrocytes in stratum radiatum of area CA1 in mouse hippocampal slices. Currents evoked by stimulation in the presence of ionotropic blockers CNQX (20 μM) and DL-APV (50 μM) revealed a current with properties consistent with glial transporters EAAT1 and EAAT2 together with a slowly decaying potassium current as previously described (Bergles & Jahr, 1997). The STC, or transporter-mediated component of the evoked current, peaked and decayed within approximately 20 ms (Figure 3.2C$_2$). The peak STC was blocked 67±10% by 30 μM L-TBA (n=4; Figure 3.2C).

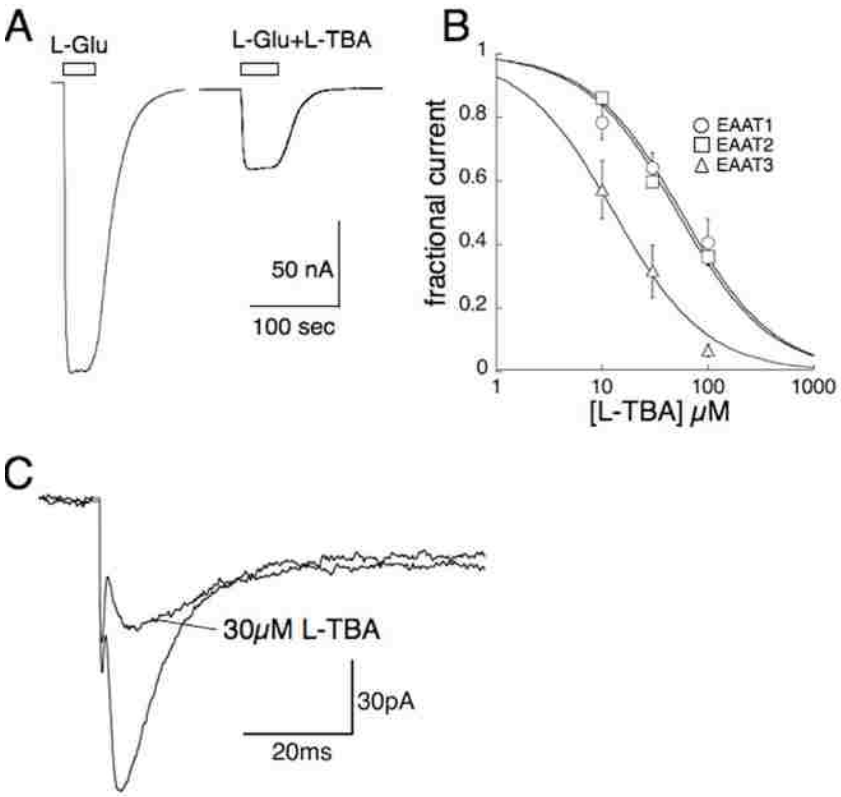

Figure 3.2. Effects of L-TBA on native and recombinant transporters. (A) Effect of 30μM L-TBA on synaptically activated transport current (STC) in hippocampal CA1 astrocyte. (A_1) Currents in the presence or absence of L-TBA were evoked by stimulation in stratum radiatum in the continuous presence of ionotropic receptor antagonists (see methods). (A_2) Subtracted current (control - L-TBA). 30μM L-TBOA blocked 66.7±10.4 of the peak STC (n=4). (B) Representative recording from voltage-clamped Xenopus oocyte expressing astrocyte transporter subtype EAAT2. 100 μM L-TBA partially blocks equimolar L-Glu uptake current mediated by EAAT2. (C) Summary of L-TBA concentration-dependence of block of 100 μM L-Glu currents in oocytes expressing EAAT1-3, showing approximately four-fold selectivity for EAAT3 by least-squares minimized fits to mean data generating IC_{50} values of 56, 52, and 13 μM, respectively.

Effects of TBA on fast excitatory synaptic transmission

Because the potential actions of L-TBA on ionotropic glutamate receptors have not been examined, its functional effects on receptor currents recorded in outside-out patches from CA1 pyramidal neurons were first evaluated. Fast application of 100 μM L- Glu alone induced robust AMPAR and NMDAR currents, while application of 100 μM L-TBA alone failed to induce measurable currents (Figure 3.3). Co-application of 100 μM L-TBA showed no antagonism of

the AMPAR (101.2±2.0% of control; n=4; p>0.6) or NMDAR currents (98.7±2.3% of control; n=5, p=0.59; Fig. 3.3C) induced by 100 μM L-Glu.

The amplitude of fEPSPs elicited by .05 Hz stimulation in stratum radiatum was not affected by application of 30 μM L-TBA (100±3% of control; n=41 slices). There was also no significant change in the 50 ms paired-pulse facilitation of the peak amplitude of fEPSPs induced by L-TBA (control, 1.72±.03; TBA, 1.60±.08; p>.05). In whole cell voltage clamp recordings from CA1 pyramidal neurons, the effect of L-TBA on EPSC kinetics was highly [Mg^{2+}]-dependent (Figure 3.4).

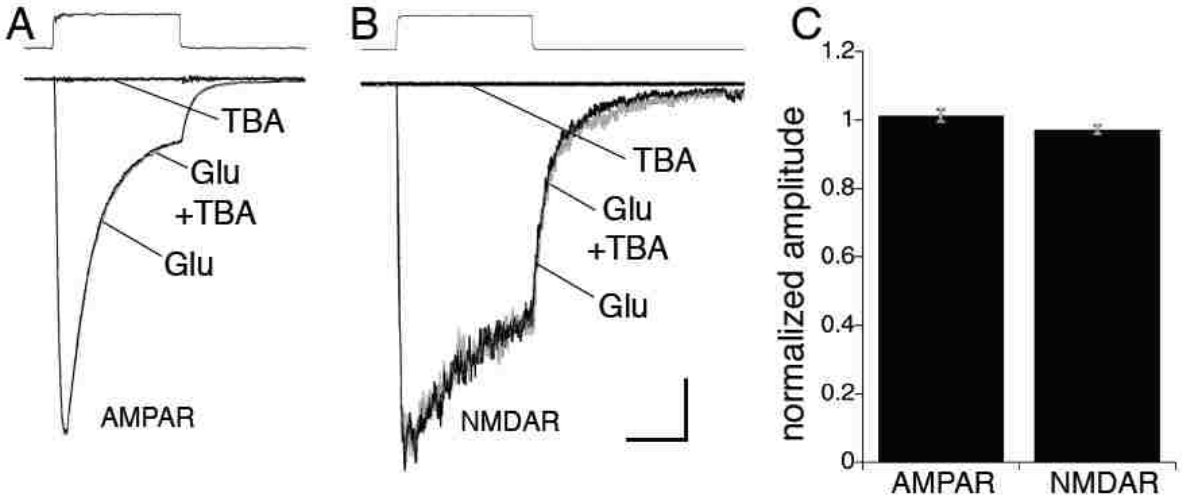

Figure 3.3. Representative recordings from outside-out patches excised from CA1 pyramidal neurons illustrating AMPAR and NMDAR responses to rapid application of 100 μM L-glutamate and/or 100μM L-TBA for durations indicated by solution exchange traces above. Responses at -60mV showing lack of agonist or antagonist actions of L-TBA on AMPARs (A; with 1.2 mM Mg^{2+}) and NMDARs (B; with 0 mM Mg^{2+}/20μM glycine/20μM CNQX). Scale bars are 50/200 ms and 50/100 pA for AMPAR/NMDAR responses respectively. (C) Summary of mean effects of 100μM L-TBA on 100μM L-Glu AMPAR and NMDAR responses.

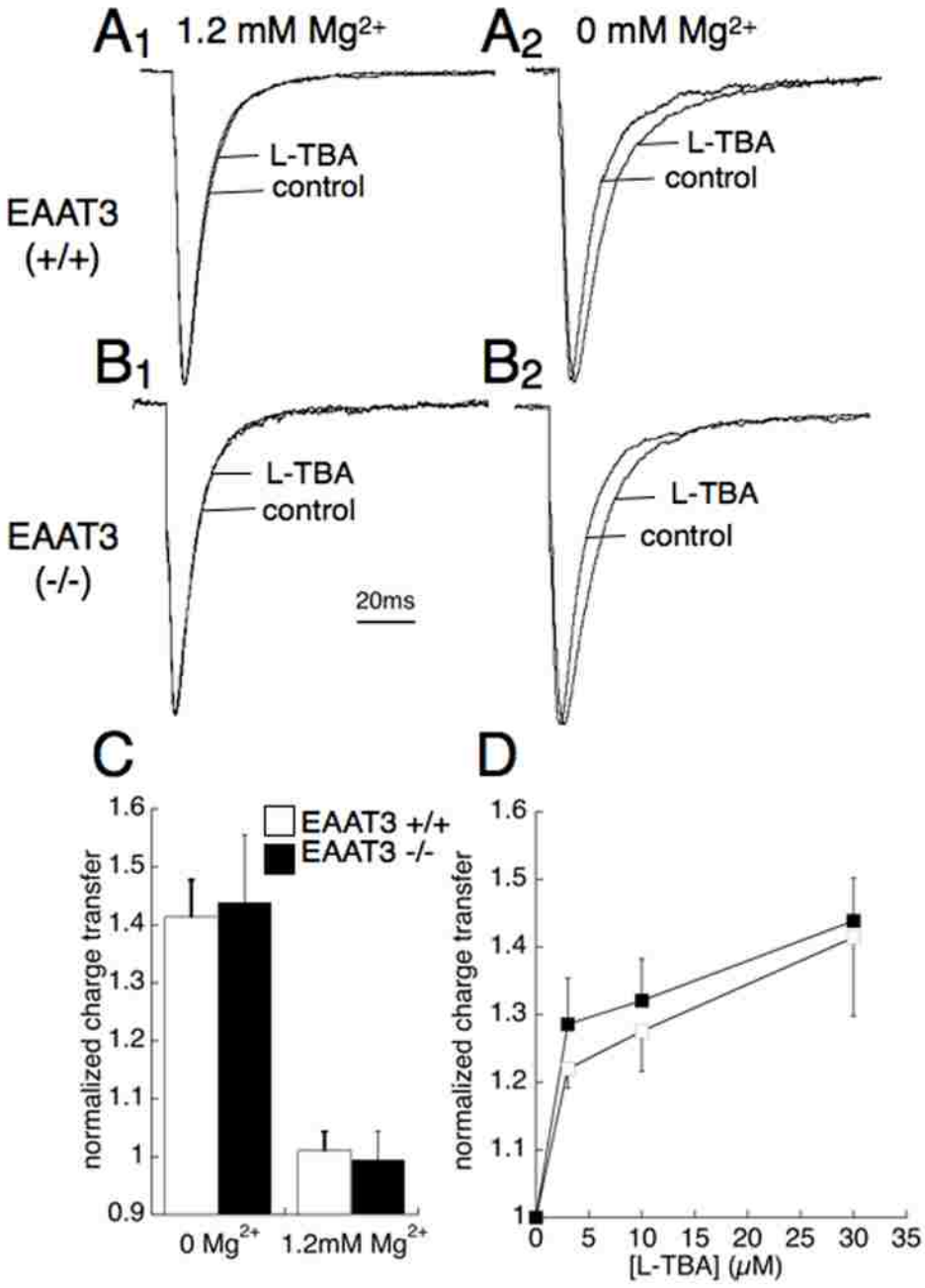

Figure 3.4. Actions of L-TBA (30 μM) on postsynaptic responses at the CA1 Schaffer collateral-pyramidal neuron synapse of EAAT3 +/+ (A) and EAAT3 -/- (B) mice. Representative whole cell recordings (-60 mV) showing effect of L-TBA on EPSCs evoked by stimulation in stratum radiatum in the presence (A_1, B_1) and absence (A_2, B_2) of physiological extracellular Mg^{2+} (1.2 mM). (C) Summary of data showing EPSC charge transfer increase in slices from EAAT3 (+/+) and (-/-) mice by 30 μM L-TBA in the absence and presence of Mg^{2+} (n=5-7 slices; $p<0.05$). (D) Summary of data showing statistically identical L-TBA concentration-dependence of EPSC charge transfer increase (normalized to control) for EAAT3 +/+ (open squares) and EAAT3 -/- (filled squares) (n=4).

In Mg^{2+}-free ACSF, 30 μM L-TBA significantly prolonged evoked EPSCs. The charge transfer in the presence of L-TBA was 141±6% of that without drug (n=6; p<.05), with no significant effect on the peak amplitude (102±7% of control, n=6). The effect of L-TBA on EPSC kinetics was presumed to be mediated by NMDAR activity, because in the presence of physiological (1.2 mM) Mg^{2+}, 30 μM TBA had no effect on the time course of the EPSC (charge transfer 101±3%; p=.78, n=4; Fig.$4A_1$). The prolongation was also not seen in the presence of 50 μM DL-APV in the absence of Mg^{2+} (data not shown). The effects of L-TBA on the EPSC charge transfer were concentration-dependent and not statistically different for EAAT3 (+/+) and EAAT3 (-/-) mice (Figure 3.4C,D).

Extracellular recording in the presence of physiological (1.2 mM) Mg^{2+} revealed an effect of L-TBA on fEPSP kinetics that exhibited pronounced frequency-dependence. 30 μM L-TBA slightly prolonged fEPSPs elicited by low-frequency (.05Hz) stimulation, while time-integrals of fEPSPs recorded during a brief 20Hz burst prolonged the time course of the fEPSP significantly further (Figure 5; 31±7% vs 69±21% for the first and second fEPSPs, respectively, n=9, p=.02). Increasing stimulus strength to increase the fEPSP magnitude by an amount comparable to the frequency facilitation had no effect on the time course of the fEPSP (data not shown). The L-TBA-induced prolongation at both low and high frequencies was not observed in the presence of 50 μM APV (Figure 3.5).

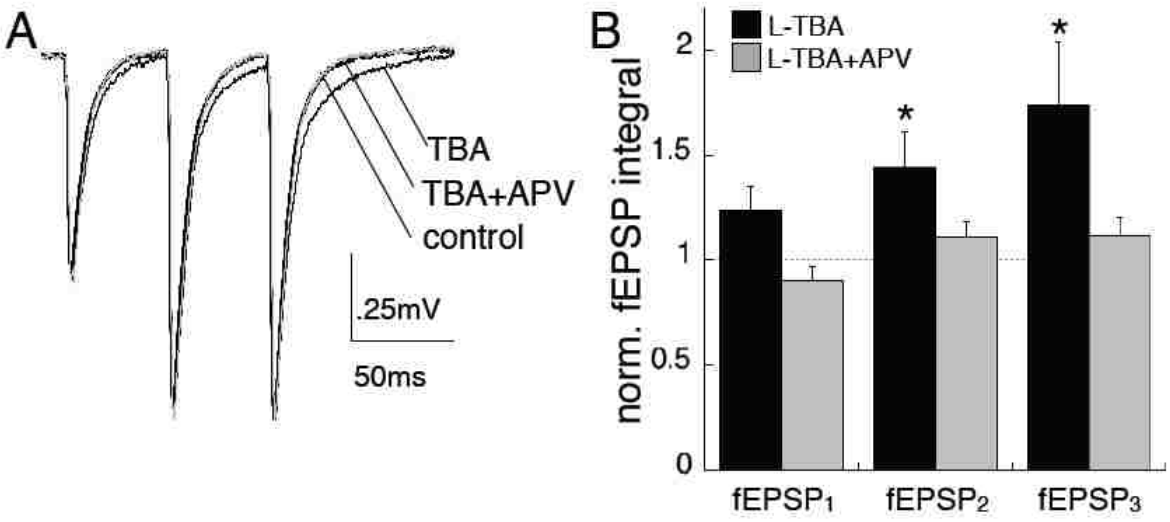

Figure 3.5. Actions of L-TBA on field responses at the CA1 Schaffer collateral-pyramidal neuron synapse. (A) Representative field EPSPs elicited in response to three stimuli delivered at 20 Hz in stratum radiatum. 30 μM L-TBA (black trace) prolonged fEPSPs relative to control (gray trace) in an activity-dependent manner (p=0.02). The TBA prolongation was inhibited by co-application of 50μM DL-APV (2nd black trace). (B) Summary of effects on fEPSP time-integrals elicited by 1, 2 and 3 stimuli normalized to corresponding fEPSPs in control ACSF (*p<.05 paired t-test; n=9 slices for one and two stimuli, n=5 slices for three stimuli).

Discussion

Selective glutamate uptake blockers are critical tools for studying the roles of glutamate transporters in modulating synaptic activity (Asztely et al., 2007; Lozovaya et al., 1999; Diamond, 2001; Arnth-Jensen et al., 2002; Scimemi et al. 2009). Both the widely used DL-TBOA and the newer analog characterized in this study are ß-substituted aryl aspartate analogs. The data presented demonstrate that L-TBA is selective for glutamate transporters over ionotropic glutamate receptors expressed on pyramidal neurons, as it neither antagonized ionotropic receptor responses to equimolar glutamate nor activated responses at concentrations up to 100μM. Unlike TBOA, TBA lacks an ether linkage between the aryl group and the amino acid, resulting in a slight change in distance and bond angle of the benzyl ring relative to the aspartyl group (Figure 2A). The computationally predicted docking orientation of L-TBA was similar to

the reported structure of L-3-Br-TBOA complexed with the archaeal homolog Glt_{Ph} (Boudker et al., 2007), with key electrostatic interactions involving R447 and D444 in TMD7 of EAAT3. Predicted interactions of the benzyl group with hydrophobic regions of EAAT3 were also in agreement with the structure of L-3-Br-TBOA complexed with Glt_{Ph}. In this conformation, the blocker prevents closure of the extracellular-facing HP2 loop which normally occludes bound L-aspartate (Yernool et al. 2004). Interestingly, a distinct orientation was predicted for L-TBOA because of the alternate interaction of R447 with the ether oxygen of L-TBOA. This interaction preserves the α-amino group interaction with D444 but causes the benzyl group to rotate to an orientation perpendicular to the membrane plane, fitting into a hydrophobic domain bordered by TMDs 7/8 and HP2 (Figure 3.2B). These predicted conformations suggest that the HP2 loop position in the L-TBA and L-TBOA transporter complexes may slightly differ. In terms of transporter selectivity, L-TBOA and L-TBA exhibit moderate selectivity for the the glial EAAT2 and neuronal EAAT3 subtypes, respectively (Shimamoto et al., 2000; Esslinger et al., 2005). While L-TBA and DL-TBOA differ in subtype selectivity, each exhibits significant subtype cross-reactivity at concentrations typically used. Because the effects of L-TBA on EPSC and fEPSP kinetics observed in this study were not significantly different in wild-type and transgenic mice lacking the EAAT3 gene, we conclude that they were primarily mediated by inhibition of glial transporters EAAT1 and/or EAAT2, which would be predicted to be approximately 75% occupied at the inhibitor concentration used (30μM) based on the K_D values of 12 μM and 9 μM for EAAT1 and EAAT2, respectively. This prediction is consistent with the 67±10% observed block of the peak synaptic transporter currents in astrocytes by L-TBA. While the glial transporter-dependent effects of L-TBA in increasing synaptic glutamate reaching NMDARs appear to dominate the results we observed, it is important to note that the selective loss of neuronal transport has been reported to result in changes in both synaptic transmission and plasticity that were not addressed here (Diamond, 2001; Scimemi et al., 2009).

Past work has generally examined transporter control of extrasynaptic glutamate spillover onto NMDARs under voltage clamp by examining the effect of transporter block on

EPSCs elicited under conditions where NMDAR activity is enabled (i.e. depolarized potentials or Mg^{2+}-free solution). Consistent with work from several groups (Asztely et al., 2007; Lozovaya et al., 1999; Diamond, 2001; Arnth-Jensen et al., 2002; Scimemi et al. 2009), we found that EAAT inhibition significantly prolonged EPSCs recorded at the Schaffer-CA1 pyramidal cell synapse in Mg^{2+}-free conditions due to enhanced NMDAR signaling. L-TBA had no effect on postsynaptic responses in voltage clamp conditions with NMDARs blocked by physiological [Mg^{2+}]. Because voltage-dependent Mg^{2+} block of NMDARs is dynamic during synaptic transmission, gaining greater insight into the role of glutamate transport in modulating synaptic activity will require the use of selective transport blockers in physiological conditions without voltage clamp. In this study we have begun to address this issue and have shown that NMDAR-mediated components of fEPSPs can be isolated that are dependent on glutamate transporter activity in a frequency-dependent manner. The effect of L-TBA on the kinetics of fEPSPs elicited by low-frequency stimulation in physiological Mg^{2+} was increased during brief bursts of higher frequency synaptic activity, and this prolongation was blocked by the NMDAR antagonist APV. This effect was not likely to be due simply to frequency-facilitation of transmitter release, because increasing stimulus strength did not affect the kinetics of fEPSPs elicited by low frequency stimulation. The data suggest that the influence of glial glutamate transporters on NMDAR signaling are likely to vary with synaptic frequency through postsynaptic voltage responses. A deeper quantitative understanding of the role of glutamate transporters in excitatory synaptic transmission will require further studies accounting for these variables.

References

Arnth-Jensen N, Jabaudon D, Scanziani M (2002) Cooperation between independent hippocampal synapses is controlled by glutamate uptake. Nat. Neurosci 5:325-331

Asztely F, Erdemli G, Kullmann DM (1997) Extrasynaptic glutamate spillover in the hippocampus: dependence on temperature and the role of active glutamate uptake. Neuron 18:281-293

Bendahan A, Armon A, Madani N, Kavanaugh MP, Kanner BI (2000) Arginine 447 plays a pivotal role in substrate interactions in a neuronal glutamate transporter. J Biol Chem 275:37436-42

Bergles DE, Jahr CE (1997) Synaptic activation of glutamate transporters in hippocampal astrocytes. Neuron 19:1297-1308

Boudker O, Ryan RM, Yernool D, Shimamoto K, Gouaux E (2007) Coupling substrate and ion binding to extracellular gate of a sodium-dependent aspartate transporter. Nature 445:387-93

Bridges RJ (2005) The substituted aspartate analogue L-ß-threo-benzyl-aspartate preferentially inhibits the neuronal excitatory amino acid transporter EAAT3. Neuropharmacology 49:850-61

Diamond JS (2001) Neuronal glutamate transporters limit activation of NMDA receptors by neurotransmitter spillover on CA1 pyramidal cells. J. Neurosci 21:8328-8338

Esslinger CS, Agarwal S, Gerdes J, Wilson PA, Davis ES, Awes AN, O'Brien E, Mavencamp T, Koch HP, Poulsen DJ, Rhoderick JF, Chamberlin AR, Kavanaugh MP, Bridges RJ. (2005) The substituted aspartate analogue L-beta-threo-benzyl-aspartate preferentially inhibits the neuronal excitatory amino acid transporter EAAT3. Neuropharmacology.49(6):850-61.

Holley DC, Kavanaugh MP (2009) Interactions of alkali cations with glutamate transporters. Philos Trans R Soc Lond B Biol Sci 364:155-61

Isaacson JS, Nicoll RA (1993) The uptake inhibitor L-trans-PDC enhances responses to glutamate but fails to alter the kinetics of excitatory synaptic currents in the hippocampus. J Neurophysiol 70:2187-91

Lehre KP, Danbolt NC (1998) The number of glutamate transporter subtype molecules at glutamatergic synapses: chemical and stereological quantification in young adult rat brain. J. Neurosci 18:8751-8757

Lozovaya NA, Kopanitsa MV, Boychuk YA, Krishtal OA (1999) Enhancement of glutamate release uncovers spillover-mediated transmission by N-methyl-D-aspartate receptors in the rat hippocampus. Neuroscience 91:1321-1330

Sarantis M, Ballerini L, Miller B, Silver RA, Edwards M, Attwell D (1993) Glutamate uptake from the synaptic cleft does not shape the decay of the non-NMDA component of the synaptic current. Neuron 11:541-549

Scimemi A, Tian H, Diamond JS (2009) Neuronal transporters regulate glutamate clearance, NMDA receptor activation, and synaptic plasticity in the hippocampus. J. Neurosci 29:14581-14595

Shimamoto K, Lebrun B, Yasuda-Kamatani Y, Sakaitani M, Shigeri Y, Yumoto N, Nakajima T (1998) DL-threo-ß-benzyloxyaspartate, a potent blocker of excitatory amino acid transporters. Mol. Pharmacol 53:195-201

Shimamoto K, Shigeri Y, Yasuda-Kamatani Y, Lebrun B, Yumoto N, Nakajima T (2000) Syntheses of optically pure ß-hydroxyaspartate derivatives as glutamate transporter blockers. Bioorg. Med. Chem. Lett 10:2407-2410

Teichman S, Kanner BI (2007) Aspartate-444 is essential for productive substrate interactions in a neuronal glutamate transporter. J. Gen. Physiol 129:527-539

Tong G, Jahr CE (1994) Block of glutamate transporters potentiates postsynaptic excitation. Neuron 13:1195-203

Tsukada S, Iino M, Takayasu Y, Shimamoto K, Ozawa S (2005) Effects of a novel glutamate transporter blocker, (2S, 3S)-3-[3-[4-(trifluoromethyl)benzoylamino]benzyloxy]aspartate (TFB-TBOA), on activities of hippocampal neurons. Neuropharmacology 48:479-491

Tzingounis AV, Wadiche JI (2007) Glutamate transporters: confining runaway excitation by shaping synaptic transmission. Nat. Rev. Neurosci 8:935-947

Yernool D, Boudker O, Jin Y, Gouaux E (2004) Structure of a glutamate transporter homologue from Pyrococcus horikoshii. Nature 431:811-8

CHAPTER 4 :EFFECTS OF SYNAPTIC FREQUENCY AND GLUTAMATE TRANSPORT ON NMDA RECEPTOR ACTIVITY AT THE SCHAFFER-CA1 SYNAPSE

Weinan Sun*, Katie M. Hoffman*, and Michael P. Kavanaugh

*these authors contributed equally to this work

Glutamate transporters are thought to help maintain synapse specificity by limiting spillover of glutamate. In the CA1 region of hippocampus, inhibition of glutamate transport has been shown to cause increased NMDAR activation in conditions preventing voltage-dependent Mg^{2+} block, but the roles of glutamate transport during normal synaptic transmission are less well understood. In this work we find that similar to inhibiting transport in the absence of Mg^{2+}, increasing release site density prolongs the time course of EPSCs and fEPSPs by increasing NMDAR activation. These effects are not seen during low frequency activity in the presence of physiological extracellular Mg^{2+} concentrations. In normal physiological conditions, the NMDAR component of the fEPSP is selectively enhanced by brief bursts of activity through a mechanism distinct from presynaptic facilitation of transmitter release. The frequency-dependence of the NMDAR facilitation matches the decay kinetics of Mg^{2+}-blocked NMDAR channels in patches from CA1 pyramidal neurons monitored with depolarizing voltage pulses. Inhibition of glutamate transport increased the amplitude and prolonged the interpulse interval-dependence of the the NMDAR-selective frequency facilitation. The data suggest that at low frequencies, Mg^{2+} block rather than glutamate transport plays a dominant role in restricting extrasynaptic NMDAR activity, but that a pool of glutamate-bound and Mg^{2+}-blocked NMDARs can signal in a phase-shifted manner during repetitive synaptic activity at frequencies governed by channel kinetics and glutamate transport.

Introduction

Glutamate is the primary excitatory neurotransmitter in the CNS, and following synaptic release it diffuses and binds to a variety of ligand-gated ion channels and G-protein coupled receptors with differing affinities and spatial distributions. In addition to these targets,

synaptically released glutamate also interacts with glutamate transporters as it diffuses through the extracellular space. Five major subtypes of excitatory amino acid transporters exist in the CNS, and three of these (EAAT1-3; also known as GLAST, GLT1, and EAAC1) are expressed in forebrain with primary distribution patterns on astrocytes (EAAT1/2) and neurons (EAAT3), respectively (Furuta et al. 1997). Studies with glutamate transporter blockers indicate that the transporters play key roles in controlling glutamate homeostasis in the CNS and in some synapses transporters modulate the dynamics of fast ionotropic glutamate receptor signaling during synaptic transmission (Marcaggi and Attwell, 2004; Tzingounis and Wadiche, 2007). A general consensus from work at the hippocampal Shaffer-CA1 pyramidal synapse is that transporter activity does not acutely modify synaptic AMPAR signaling (Isaacson and Nicoll, 1993; Sarantis et al., 1993). However, voltage-clamp recordings of NMDAR EPSCs indicate that inhibition of glutamate transport can lead to spillover and activation of extrasynaptic NMDARs (Asztely et al., 1997; Lozovaya et al., 1999; Diamond, 2001, Arnth-Jensen et al. 2002; Tsukada et al., 2005; Scimemi et al., 2009).

A notable limitation of studies examining the influence of glutamate transport on postsynaptic NMDAR currents arises from the necessity of recording these currents in non-physiological voltage-clamp and/or Mg^{2+}-free conditions due to voltage-dependent block of the channels by Mg^{2+} (Mayer et al. 1984; Nowak et al. 1984). Previous work has shown that synaptic NMDAR signaling is likely to be strongly influenced by Mg^{2+} block and the temporal pattern of postsynaptic voltage changes (Collingridge et al., 1988). In this work we examined the influence of glutamate transport and postsynaptic activity on excitatory signaling in CA1 pyramidal neurons by recording responses in the presence and absence of extracellular Mg^{2+}. We used the selective glutamate transporter inhibitor L-threo-beta-benzylaspartate (L-TBA; Esslinger et al. 2005; Sun et al, 2011) to confirm the role of transport in restricting glutamate diffusion and binding to extrasynaptic NMDARs. In order to study the influence of transport in physiologically relevant conditions with extracellular Mg^{2+}, we examined the effects of L-TBA on the isolated AMPAR- and NMDAR-mediated components of extracellular fEPSPs. At low

frequencies of synaptic activity, glutamate transport inhibition had minimal impact on synaptic signaling, but with higher frequencies of stimulation NMDAR signaling was facilitated due to relief of Mg^{2+} block from glutamate-occupied receptors, and this effect was significantly enhanced by inhibition of glutamate transport. The data suggest that synaptic NMDAR responses are controlled by interacting factors including release frequency, glutamate transport, Mg^{2+} block, and NMDAR channel kinetics. In physiological conditions with transport intact, the threshold frequency for selective NMDAR signaling corresponds approximately to theta rhythm, which is correlated with induction of LTP.

Materials and Methods

Drugs

Drugs and chemicals were purchased from Sigma, except CNQX and DL-APV, which were from Tocris. L-TBA was synthesized and purified as described (Esslinger et al. 2005) and a stock solution was dissolved in DMSO at 50mM.

Hippocampal slice preparation and recording

CD1 mice (P15-30) were anesthetized with isofluorane and decapitated in accordance with University of Montana IACUC regulations. The brain was rapidly dissected and placed in ice-cold solution containing (in mM): 80 NaCl, 24 $NaHCO_3$, 25 glucose, 75 sucrose, 2.5 KCl, 1.25 NaH_2PO_4, 0.5 $CaCl_2$, 5 $MgCl_2$, 1 ascorbic acid, 3 Na pyruvate. The solution was saturated with 95% O_2 and 5% CO_2 (pH 7.3). 300µm thick coronal hippocampal slices were cut using a vibratome (VT1200S Leica, Germany), then hemisected and placed in artificial cerebral spinal fluid (ACSF) containing (in mM): 126 NaCl, 2.5 KCl, 1.2 $MgCl_2$, 2.4 $CaCl_2$, 1.2 NaH_2PO_4, 11.4 glucose, and 21.4 $NaHCO_3$ saturated with 95%O_2 and 5% CO_2 (pH 7.3) and maintained at

30°C. Slices were allowed at least 1 hour to recover before being placed in a submersion-type recording chamber perfused at 1.6-2.0 ml/minute with ACSF at 30°C. Slices were visualized on an upright fixed-stage microscope (Olympus BX51WI) equipped with IR-DIC optics. The recording pipettes (3-6MΩ resistance) were filled with internal solution containing (in mM): 110 Cs methanesulfonate, 38 CsCl, 10 HEPES, 10 Na-phosphocreatine, 0.1 EGTA, 0.3 Mg-ATP, 0.3 GTP, 5 QX-314, pH=7.3. Series resistance (typically 15-20 MOhm), was monitored and recording was terminated if a change >20% was observed. Holding potential was -60 to -70 mV. 100μM picrotoxin was added to the ACSF for whole-cell recordings and an incision was made between CA3 and CA1. Extracellular field excitatory post synaptic potentials (fEPSPs) were recorded using glass electrodes filled with ACSF. EPSCs and fEPSPs were induced with 100 μs current pulses between 0.1mA - 0.4mA administered through ACSF-filled stimulating pipettes placed in stratum radiatum. Recordings were made with analog-digital converters and amplifiers from Molecular Devices, and data were acquired at 20kHz and filtered at 5-10 kHz. Data were acquired and analyzed with Axograph software (version 1.1.6). EPSC charge transfer changes and fEPSP prolongation were quantified by integrating the area from the normalized peak of the response until 100 ms after the peak. EPSCs and fEPSPs were elicited with alternating single and paired stimuli at varying intervals, and the response time-integral of the second response was calculated following subtraction of the first. Data are presented as mean ± S.E. and were evaluated by Student's paired t-test or as noted.

Nucleated outside-out patch recordings

Nucleated patches were pulled from the soma of CA1 pyramidal neurons of CD1 mice (P10-12) identified under transmitted IR-DIC optics. Intracellular pipette solution contained (in mM): 60 Cs-methanesulfonate, 38 CsCl, 20 Cs_4BAPTA (4*CsOH+BAPTA), 10 HEPES, 10 Na-phosphocreatine, 4 MgATP, and 0.3 NaGTP, 5 QX-314, pH 7.3 (adjusted by HCl or CsOH). Patch recordings were made at 25°C in the presence of 20 μM CNQX. L-glutamate (1 mM) was

applied for 1 ms through a 200 μm diameter double-barreled theta tube attached to a piezoelectric bimorph. Solution exchange kinetics were estimated following patch rupture by measuring junction currents during switches between iso- and hypo-osmotic solutions as displayed above receptor current records. To investigate the kinetics of Mg^{2+}- blocked channels, 5 ms voltage pulses from -60mV to -20mV or +40mV were applied at varying intervals as indicated following the glutamate pulse. NMDAR currents were also recorded at -60 mV in Mg^{2+}-free ACSF containing 20 μM CNQX and 20 μM glycine. Control voltage jump recordings without a glutamate pulse were made to subtract leak and capacitance currents. Averages of 5-10 responses to repetitive application are shown.

Results

Mg^{2+} and transport modulation of EPSCs during enhanced glutamate release

NMDAR-mediated EPSCs at the Schaffer-CA1 pyramidal cell synapse are enhanced by spillover when glutamate transport is inhibited or when glutamate release is increased (Asztely et al., 1997; Lozovaya et al., 1999, 2004; Diamond, 2001, Arnth-Jensen et al. 2002; Tsukada et al., 2005; Scimemi et al., 2004, 2009; Sun et al., 2011). We examined the interacting influences of Mg^{2+}, frequency facilitation, and glutamate transport on EPSC kinetics. Paired-pulse stimulation (50 ms interpulse interval) facilitated the EPSC amplitude to 187 ± 10% and 185 ± 11% of the first EPSC in the presence and absence of Mg^{2+}, respectively (n=14). After normalizing peak amplitudes, control and facilitated EPSCs recorded in the presence of 1.2 mM Mg^{2+} were superimposable and the normalized charge transfer in the second EPSC was 98.9 ± 1.9% of that in the first (n=14; figure 4.1). As expected from relief of voltage-dependent Mg^{2+} NMDAR block (Nowak et al. 1984; Mayer et al. 1984), removal of Mg^{2+} prolonged EPSCs elicited by single stimuli (normalized charge transfer increased to 137 ± 6% of control; $p=0.006$; n=4) and this prolongation was significantly greater ($p<0.02$) in the facilitated EPSC (normalized

charge transfer 212 ± 22% of control; p=0.015 n=4; figure 4.1). The prolongation of the first and second EPSC after removal of Mg^{2+} was due solely to relief of block of the NMDAR response without affecting AMPAR signaling, as the prolongation in Mg^{2+}-free ACSF was completely blocked by 50 μM DL-APV (figure 4.1).

In order to examine the involvement of glutamate transport in the low frequency and frequency-facilitated NMDAR responses, we used the glutamate transporter blocker L-threo-benzylaspartate (L-TBA), an aspartate derivative with high selectivity for glutamate transporters over ionotropic glutamate receptors (Esslinger et al., 2007; Sun et al. 2011). At 30 μM, a concentration that blocks approximately 67% of the astroglial synaptic transport current in CA1 (Sun et al. 2011), L-TBA had no effect on either the control or facilitated EPSC in the presence of 1.2 mM Mg^{2+} (charge transfer 101.1±3.3% and 101.4±11.8% of control, respectively; n=4, figure 4.1). In the absence of Mg^{2+}, L-TBA prolonged both the first and second EPSCs induced by paired pulse stimulation (charge transfers increased to 141 ± 6.3% and 163 ± 9% of control, respectively; n=6; P<0.01; figure 4.1). The mean prolongation induced by L-TBA was greater in the facilitated EPSC, but this difference did not reach statistical significance (p=0.08).

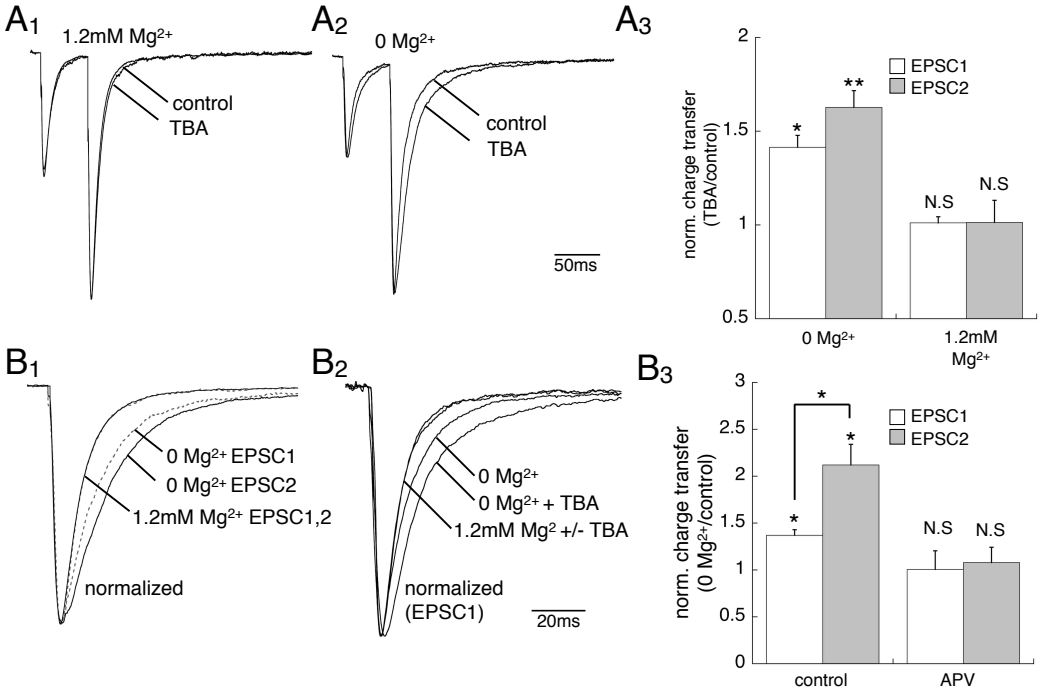

Figure 4.1. EPSC prolongation caused by transport block and/or increased release site density. (A) EPSC induced by a paired pulse stimulation in the presence or absence of 30μM TBA in ACSF containing 1.2mM Mg^{2+} (A_1) or 0 Mg^{2+} (A_2), the charge transfer of 1st and 2nd EPSC after TBA were 141.4±6.3% (B_2, n=6, p<0.01) and 162.7±8.9% (n=6, p<0.0001) of control for 0 Mg^{2+} group, 101.1±3.3% (B_2, n=4, p>0.7) and 101.4±11.8% (n=4, p>0.9) for 1.2mM Mg^{2+} group. TBA prolongation of 1st EPSC and 2nd EPSC in 0 Mg^{2+} solution are not significantly different (p=.08, A_3). (B_1) Normalized 1st and 2nd EPSC induced by a paired pulse stimulation with 50ms interpulse interval in control ACSF (containing 1.2mM Mg^{2+}) and in 0 Mg^{2+} ACSF. (B_3) Quantification of Mg^{2+} removal's effect on EPSC's time integral with presence or absence of APV.

Mg^{2+} and transport modulation of field responses to enhanced glutamate release

The above results are consistent with a number of studies indicating that facilitated glutamate release results in a significant increase in transmitter binding to NMDARs and that this binding is limited by transporter activity (Asztely et al., 1997; Lozovaya et al., 1999, 2004; Diamond, 2001, Arnth-Jensen et al. 2002; Tsukada et al., 2005; Scimemi et al., 2004, 2009; Sun et al., 2011). In addition to transport, another limiting factor in the NMDAR response is the degree of voltage-dependent Mg^{2+} block, which is dynamically controlled during synaptic transmission under physiological conditions. To investigate the role of Mg^{2+} in controlling activation of NMDARs by glutamate spillover in the absence of voltage clamp, we utilized extracellular field recording and isolated AMPAR and NMDAR contributions to fEPSPs in order to monitor the change in each as release site density and transporter activity varied. We verified that NMDAR fEPSPs could be detected by evoking responses in the presence of CNQX (10μM) and in the absence of Mg^{2+}. The remaining field response in these conditions was blocked by DL-APV (50μM), confirming that it was NMDAR-mediated (figure 4.2). In comparison with the fEPSP kinetics in physiological ACSF, the NMDAR fEPSPs isolated in the absence of Mg^{2+} displayed slower kinetics, as expected from the difference in channel kinetics and glutamate affinity between NMDARs and AMPARs (Spruston et al., 1995; Figure 2; 10-90% rise time 1.67 ± 0.15 ms n=11, 6.29 ± 0.66 ms; n=11; p<.0001). In comparison to the fEPSPs recorded in physiological Mg^{2+}, which predominantly reflect AMPAR activity, the kinetics of NMDAR fEPSPs isolated in the nominal absence of Mg^{2+} displayed a marked sensitivity to release site density

and decayed more slowly as stimulus strength was increased (figure 4.2). The normalized time-integrals of the fEPSPs in control ACSF were constant over a range of stimulus strengths, while the NMDAR fEPSP decay times increased monotonically over the same range (Figure 4.2C).

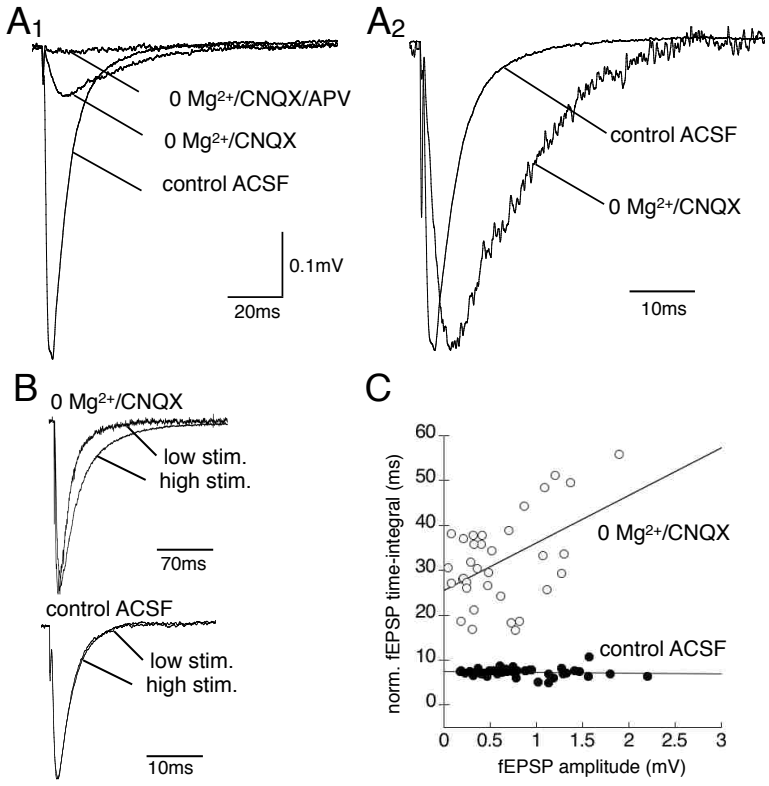

Figure 4.2. Isolated NMDAR fEPSPs at the CA3-CA1 pyramidal neuron synapse display slower decay kinetics with increasing release site density. (A_1) Bath application of 0 Mg^{2+} ACSF and 10μM CNQX isolate a NMDAR-mediated fEPSP confirmed by complete block with the NMDAR antagonist DL-APV (50μM), representative trace. (A_2) The normalized Mg^{2+}/10μM CNQX (NMDAR) fEPSP rise time is slowed and decay kinetics are prolonged as compared to the fEPSP in control ACSF (1.2mM Mg^{2+}, representative trace.) (B) upper trace: NMDAR (0 Mg^{2+}/10μM CNQX) fEPSP decay kinetics are prolonged by stimulation strength increase (from 20% to 80% of the intensity which induces pop. spike). Lower trace: Stimulation strength does not alter AMPAR/NMDAR fEPSP kinetics elicited at low frequency in the presence of Mg^{2+}. (C) Normalized fEPSP time-integral (peak to 200ms after the peak) of individual experiments in control (n=44 from 17 slices) and 0 Mg^{2+}/10μM CNQX (n=33 from 13 slices) conditions as a function of the first fEPSP amplitude and were modeled by linear regression. (The normalized time-integrals of the control fEPSPs were constant over a range of stimulus strengths r=0.076, Slope was not significantly greater than 0, p=0.65, while the NMDAR fEPSP decay times increased over the same range (Figure 2B) r=0.482, Slope was significantly greater than 0, p=0.004.)

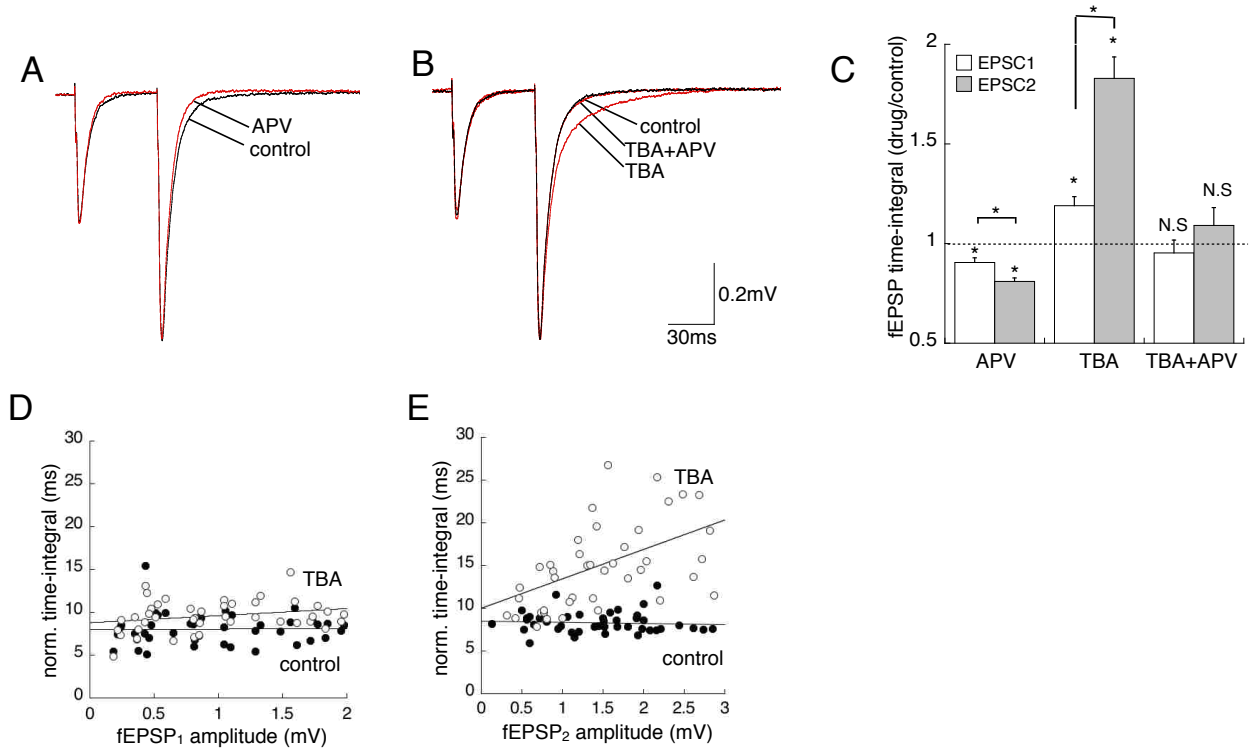

Figure 4.3. **The enhancement of NMDAR activation induced by transport block is frequency-dependent manner in physiological (non-voltage clamp, 1.2 mM Mg^{2+}) conditions. (**A) 50 μM DL-APV revealed an APV sensitive component in fEPSP. (B) 30 μM L-TBA prolonged fEPSPs in a frequency-dependent manner that was reversed by co-application of 50μM DL-APV. ((C) Summary of mean effects in 50μM DL-APV(n=44, 9 slices), 30μM TBA (n=42, 9 slices) and 50μM DL-APV and 30μM TBA (n=9, 9 slices) in a single and paired-pulse protocol; * denotes p<.05. (D, E) Field EPSP time-integral of Individual experiments (all peaks were normalized to 1, integrated from 0-200ms after peak) in control and 30μM TBA as a function of first (D) and second (E) fEPSP amplitude (n=43). (least-squares linear regression/ slope analysis L-TBA: r =.43, p=0.004; control: r = 0.076, p=0.650)

We next sought to characterize NMDAR synaptic responses in physiological conditions by isolating their contribution to the field response with 50 μM DL-APV in ACSF containing 1.2mM Mg^{2+}. In these conditions, the primary component of the Schaffer-CA1 fEPSP arises from AMPAR signaling, but 50 μM DL-APV revealed an NMDAR-mediated component of the fEPSP detectable by an increased rate of decay in its presence (figure 4.3). The change in the fEPSP kinetics induced by DL-APV was quantified by measuring the time integrals of the responses after normalizing the peak amplitudes. The NMDAR-mediated field signal was selectively enhanced relative to the AMPAR signal by paired-pulse facilitation. The normalized

peak time integrals of the first and second fEPSPs in the presence of DL-APV were 90 ± 2 and 81 ± 2% of control, respectively ($p<0.01$; n=44; figure 4.3).

Inhibition of glutamate transport by 30μM L-TBA slowed the fEPSP decay kinetics, and this effect was significantly greater in the frequency-facilitated fEPSP relative to the response elicited at low frequency ($p=.001$; Figure 4.3B,C). The effect of TBA on the fEPSP kinetics was reversed by DL-APV, suggesting that the prolongation associated with transporter inhibition was predominately mediated by NMDARs. DL-APV did not speed the frequency-facilitated fEPSP decay kinetics to the extent seen in the absence of L-TBA, suggesting that L-TBA may have a small additional effect on the kinetics of the AMPAR signal (figure 4.3B,C).

The selective increase in paired-pulse facilitation of NMDAR signaling caused by glutamate transporter inhibition could potentially involve several factors, including an increase in overall release site density due to increased presynaptic release probability (Dobrunz and Stevens, 1997), increasing multivesicular release from a subset of individual synapses (Christie and Jahr, 2006), and/or by overwhelming glutamate transport (Diamond and Jahr, 2000). To examine the effect of increased release site density, stimulus strength was varied in the presence or absence of 30μM L-TBA. In the presence or absence of L-TBA, the normalized time-integral of fEPSPs elicited by low frequency stimulation in the presence of Mg^{2+} did not change as peak amplitude varied over a range from approximately 200 μV to 2 mV (Figure 3D). This contrasts with the significant prolongation seen with increased release site density in the absence of Mg^{2+} (figure 2B). The kinetics of fEPSPs elicited at low frequency were also unchanged in the presence of L-TBA, in contrast to the effect of transport inhibition on NMDAR EPSCs in the absence of Mg^{2+} (figure 4.1B).

Unlike fEPSPs elicited at low frequency, the time-integrals of fEPSPs elicited by paired-pulse facilitation were significantly increased function of peak amplitude the presence of Mg^{2+}, inhibition of glutamate transport by 30 μM L-TBA resulted in a significant increase in the frequency-facilitated fEPSP time integral as function of peak amplitude (Figure 4.3E; least-squares linear regression L-TBA: $r =.43$, $p=0.004$; control: $r = 0.076$, $p=0.650$). In the absence of

transport inhibition, the facilitated fEPSP kinetics were unchanged by changing release site density.

Mechanism of frequency-dependent NMDAR facilitation

In order to examine the mechanism underlying the observed difference in frequency facilitation of AMPAR and NMDAR fEPSPs, we isolated NMDAR fEPSPs elicited by paired-pulse stimulation in either the presence or absence of extracellular Mg^{2+}. In the first set of experiments, NMDAR responses were isolated by recording fEPSPs in control ACSF containing 1.2mM Mg^{2+} and subtracting responses in the presence of 50 μM APV. In the latter case, NMDAR fEPSPs were recorded in extracellular solution containing 20 μM CNQX with 0 Mg^{2+} (see Figure 4.2). The peak amplitude facilitation ratios of the compound fEPSP in control ACSF, the AMPAR-mediated fEPSP recorded in the presence of 50μM APV, and the NMDAR fEPSP recorded with CNQX in the absence of Mg^{2+} were not significantly different (Figure 4.4A-C). In contrast, the facilitation ratio of the NMDAR fEPSP isolated by APV during recording in physiological ACSF with Mg^{2+} was significantly greater (Figure 4.4D,E; $p<.001$).

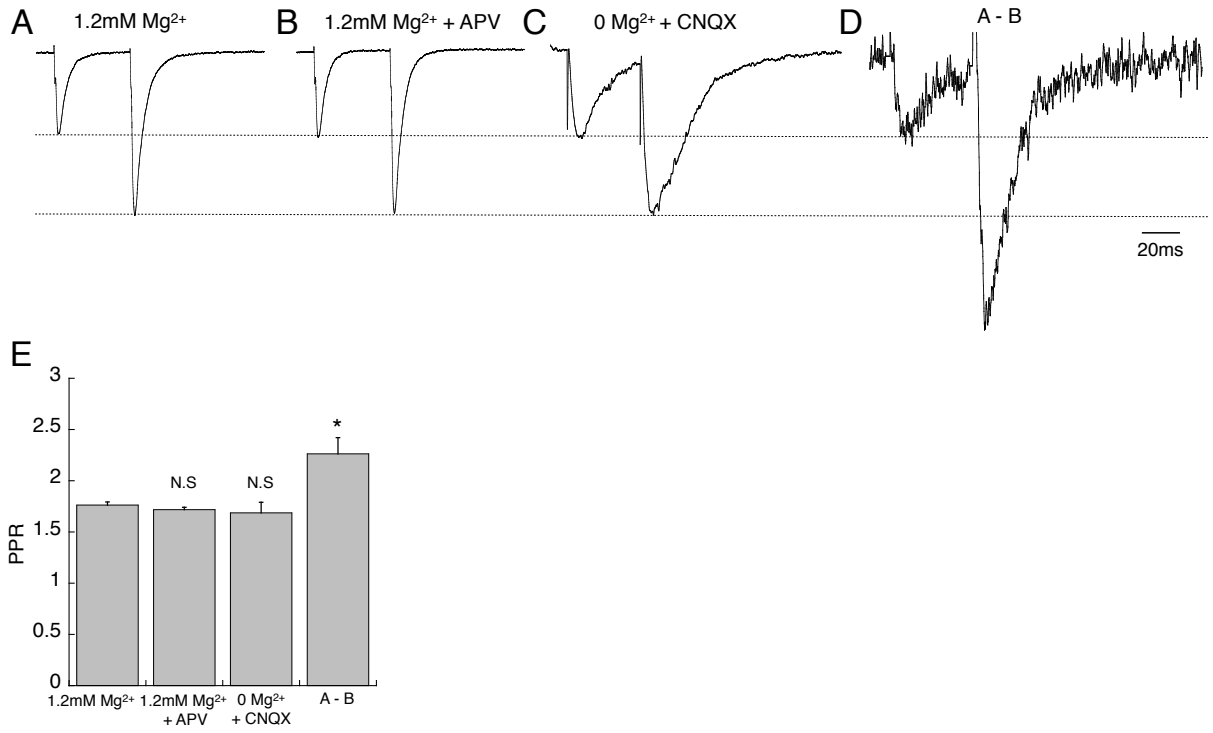

Figure 4.4. Paired pulse facilitation of NMDAR at the CA3-CA1 pyramidal neuron synapse in the presence and absence of 1.2 mM Mg^{2+}. Paired-pulse fEPSPs (50 ms interval, normalized to first peak) of (A) fEPSP in control ACSF (B) AMPAR (50μM DL-APV), (C) NMDAR Mg-free +10μM CNQX, and (D) Physiological NMDAR (control-APV), (E) Quantification of paired pulse ratio under different conditions.

These data suggested the possibility that selective enhancement of NMDAR signaling during repetitive activity may be due to a postsynaptic effect of Mg^{2+}. To compare the interpulse interval-dependence of the NMDAR facilitation with that of the presynaptic release change reflected in facilitation of the AMPAR fEPSP, paired stimuli were delivered at varying interpulse intervals (Figure 4.5). The time-dependent facilitation of the NMDAR signal was compared to that of the AMPAR signal, and the time-dependence of their mean relative amplitudes revealed that the NMDAR-selective frequency-enhancement decayed with a time constant of 238 ms (Figure 4.5B). We used the same analysis to compare the interpulse interval-dependence of the NMDAR signal isolated in the absence of Mg^{2+} with CNQX with the AMPAR signal. In this case,

the facilitation ratios and their frequency dependence were not different (Fig. 4.5C,D), suggesting a key role for physiological Mg^{2+} in generating the time course of NMDAR-selective frequency facilitation.

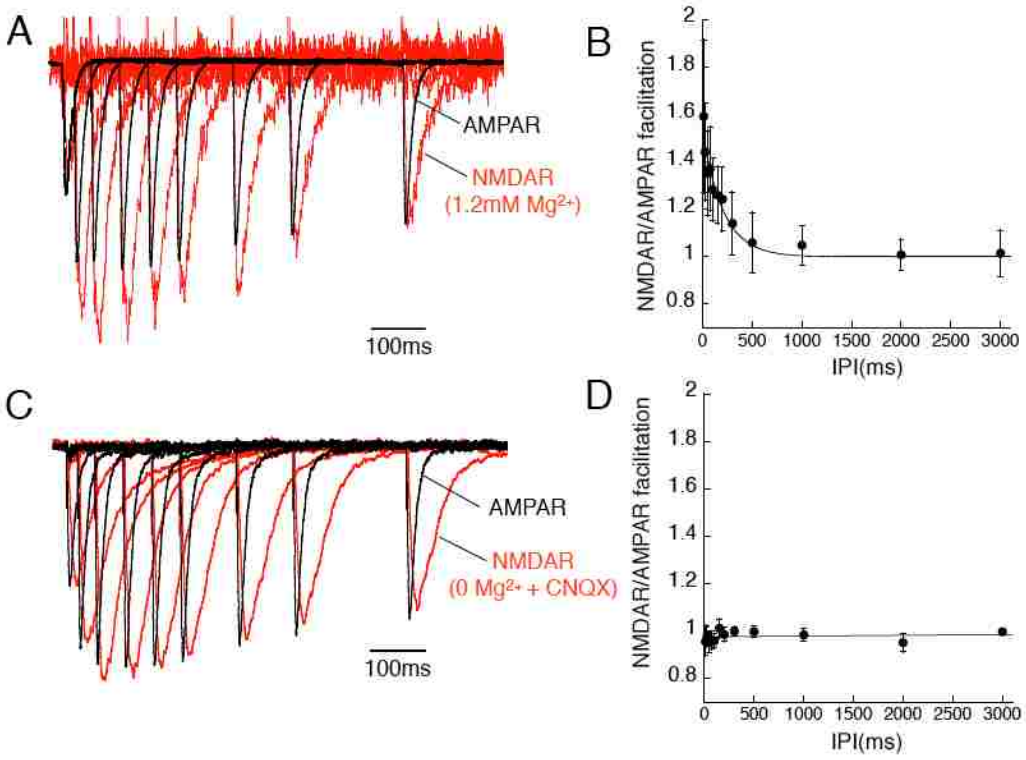

Figure 4.5. Physiological NMDAR signaling is limited by glutamate transport in a frequency- and Mg^{2+}-dependent manner at the the CA3-CA1 pyramidal neuron synapse. (A) Normalized APV-sensitive component of the total fEPSP in the presence of 1.2mM Mg^{2+} (control - APV; red traces) AMPAR fEPSPs (black traces). (B) Summary of ratios of physiological NMDAR PPR (control-APV) and AMPAR PPR (n=9). Data points were fit to a single exponential decay function (time constant: 208ms) (C) Normalized NMDAR fEPSP recorded in 0 Mg^{2+} and 10μM CNQX overlaid with AMPAR fEPSPs (black traces). (D) Summary of ratios between NMDAR PPR (0 Mg^{2+} /10μM CNQX) and AMPAR PPR (n=6) .

Frequency- and Mg^{2+}-dependent enhanced synaptic NMDAR signaling correlates with channel deactivation/desensitization kinetics

NMDAR receptors display slow decay kinetics following glutamate binding (Lester and Jahr, 1992; Spruston et al., 1995;). We sought to test the possibility that Mg^{2+} played a role in the NMDAR-selective frequency facilitation through voltage-dependent unblock of receptors occupied by a previous synaptic glutamate transient. We compared the paired-pulse interval-dependence of this synaptic facilitation with the time-dependence of responses to brief voltage pulses relieving Mg^{2+} unblock from NMDAR channels in outside-out patches at varying intervals following exposure to a transient glutamate concentration jump. In nucleated patches from visualized CA1 pyramidal neurons, the response to 5 ms voltage jumps relieving Mg^{2+} block slowly decayed as a function of the time interval following a 1ms exposure to 1 mM L-Glu (Figure 4.6). The decay time course of the currents matched the time-interval dependence of the synaptic facilitation reasonably well, with a fast time constant 148±12ms and a slow time constant of 521±73ms, mean single exponential fitting time constant was 227ms (Figure 4.6 inset).

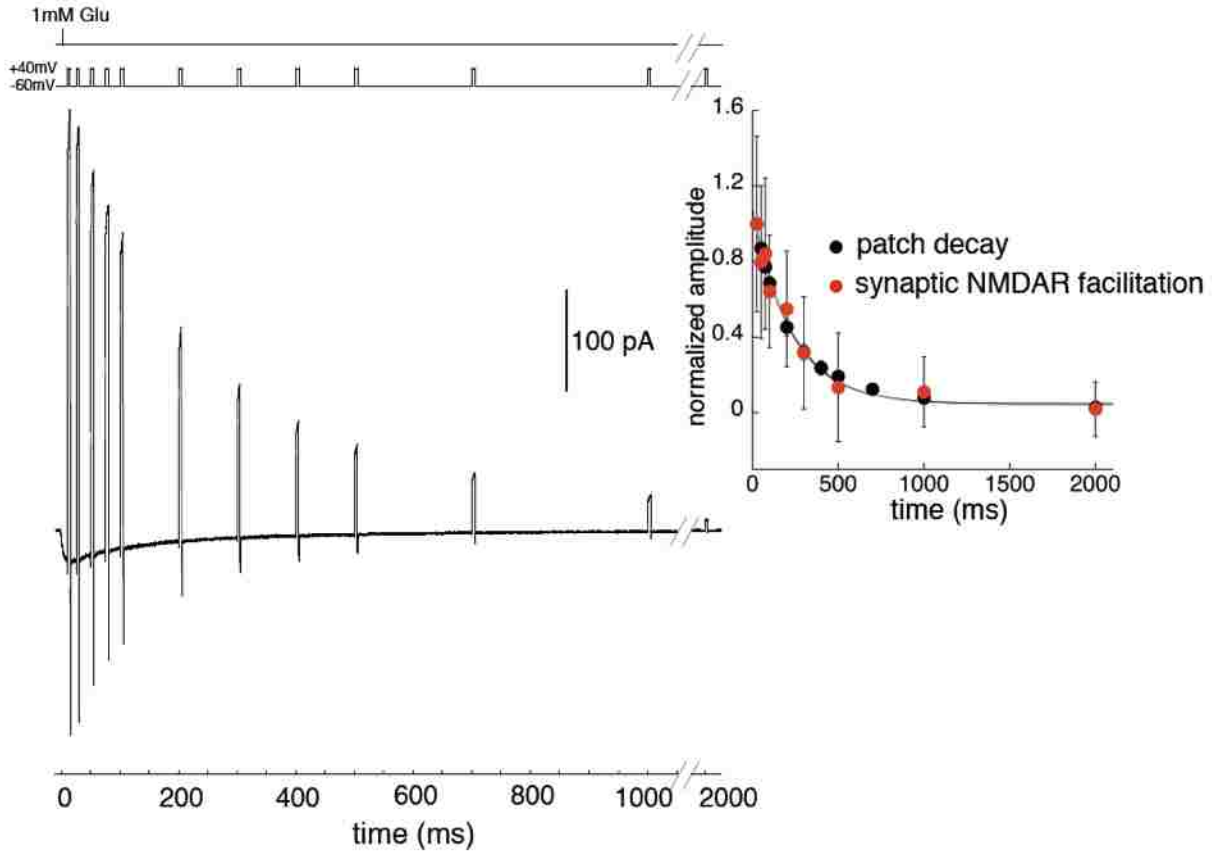

Figure 4.6. Determining glutamate unbinding rate using nucleated patch recording. Voltage jump induced NMDAR currents recorded from outside out patches with 1ms L-Glu application. Inset: Single exponential fitting of decay kinetics. Black dots, decay of voltage jump currents from outside out patches. Red dots, decay kinetics of normalized APV sensitive fEPSP.

Glutamate transport block alters the frequency-dependent NMDAR facilitation

As indicated in figure 1 and 3, glutamate transport block significantly increase the occupancy of glutamate molecules on NMDAR after glutamate release. We thus tested the effect of transport block on the frequency dependent NMDAR facilitation. With 30μM TBA, the paired-pulse interval-dependence facilitation of NMDAR was significantly increased and prolonged compared to the facilitation time course in control condition. This facilitation exhibits a double exponential profile, with a fast tau 280ms and a slow tau of 3791ms (Fig. 4.7)

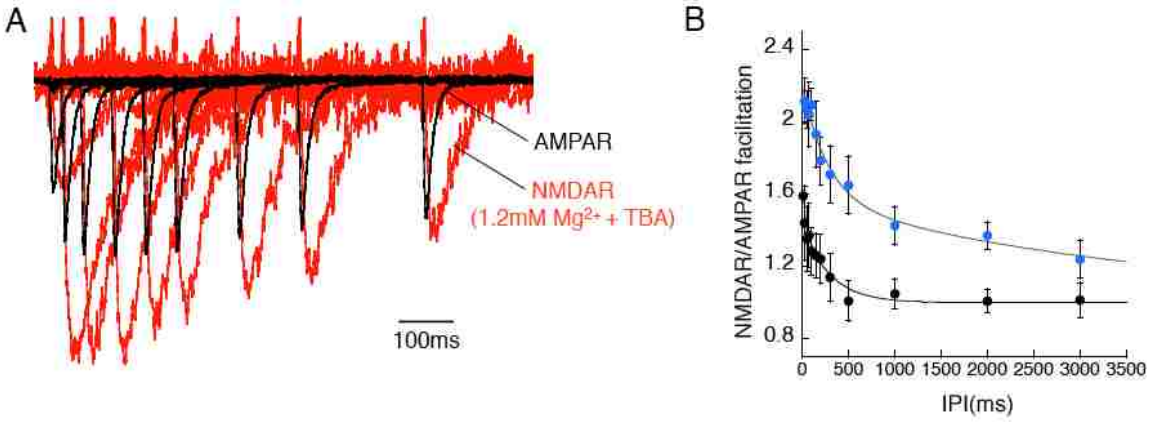

Figure 4.7. TBA's effect on frequency facilitation of NMDAR fEPSPs. (A) NMDAR component of the fEPSP (red traces) and AMPAR fEPSP (black traces) in the presence of 1.2mM Mg^{2+} and 30μM TBA at interpulse intervals from 0 to 500ms (40 traces mean trace n=4). (B) Summary of ratios between NMDAR PPR (1.2mM Mg^{2+}) and AMPAR PPR (n=6) with the presence of 30μM TBA (blue dots, double exponential fit: fast: 280ms slow: 3791ms).

Discussion

Significant uncertainty surrounds the role of glutamate transport in modulating postsynaptic receptor responses, in part because the effects of uptake inhibition in CNS are region-dependent. The use of transport blockers that vary in selectivity and mechanism may also contribute to heterogenous effects observed (see Tzingounis and Wadiche 2007). A general consensus emerging from work at the hippocampal Shaffer-CA1 pyramidal synapse is that transporter activity does not acutely modify synaptic AMPAR responses (Isaacson and Nicoll, 1993; Sarantis et al., 1993; but see Tong and Jahr, 1996), while inhibition of transport or increasing presynaptic release leads to glutamate spillover and activation of extrasynaptic NMDAR receptors (Asztely et al., 1997; Lozovaya et al., 1999; Diamond, 2001, Arnth-Jensen et al. 2002; Scimemi et al., 2009). The central evidence for this conclusion comes from voltage clamp recordings of EPSCs under conditions where NMDAR activity is enabled, i.e. depolarized potentials or Mg^{2+}-free solution (Mayer et al. 1984). An important limitation of voltage clamp in analyzing the influence of transport on synaptic responses arises because of the potential interplay between the kinetics of glutamate spillover and dynamic voltage changes influencing Mg^{2+} block of NMDARs. This is exemplified by the strong effects of postsynaptic voltage and Mg^{2+} on frequency-facilitation of NMDAR-dependent responses (Herron et al. 1986; Collingridge et al. 1987).

The results of this study show that fEPSPs resulting from low frequency (<.1 Hz) stimulation are virtually entirely mediated by AMPAR signaling, and that NMDAR signaling is only detected during brief repetitive activity involving as few as two stimuli at 5-10 Hz (Figure 4.3). This frequency-dependent prolongation of fEPSPs through activation of NMDAR signaling occurred in physiological conditions with transport intact, and it was significantly enhanced by glutamate transport inhibition. During low frequency synaptic activity, however, inhibition of transport had minimal effect on fEPSP kinetics. In general, these results suggest that a

threshold for repetitive synaptic activity at approximately 5 Hz acts as a control switch for NMDAR signaling, and glutamate transport modulates the signal (Figure 4.5 and 4.7).

The interacting effects of frequency and transport on NMDAR signaling could theoretically arise in several ways. First, an increase in release probability throughout a frequency-facilitated set of inputs will result in an increase in the overall density of active release sites, which could tend to slow clearance and promote signaling through pooling of transmitter between sites (Otis et al. 1996). Consistent with previous work (Diamond, 2001; Arnth-Jensen et al., 2002), raising release site density by increasing stimulation intensity leads to enhanced transmitter binding to NMDARs, as directly revealed by NMDAR responses in permissive Mg^{2+}-free conditions (Figure 4.2B upper trace). In the presence of 1.2 mM [Mg^{2+}], however, NMDAR signaling is not detectable over a range of stimulus strengths (Figure 4.2B lower trace). This suggests that the NMDAR signaling revealed by APV in frequency-facilitated fEPSPs recorded in physiological ACSF cannot be solely due to increased release site density. In addition to increasing release site density, presynaptic frequency facilitation can lead to increased synaptic glutamate concentrations by increasing the probability of multi-vesicular release at the Shaffer-CA1 pyramidal cell synapse (Christie and Jahr, 2006). This is also not likely to be a major factor in enhanced NMDAR signaling, however, because enhancement of multi-vesicular release at low frequencies by elevating extracellular [Ca^{2+}] does not prolong NMDAR EPSCs, although it does enhance the prolongation caused by glutamate transport inhibition (Christie and Jahr, 2006). Another piece of evidence that distinguishes the mechanism of the frequency-dependent NMDAR signaling from presynaptic facilitation is that NMDAR responses increased with longer pulse trains, unlike the AMPA response facilitation (Figure 4.3). A third frequency-dependent mechanism that could in principle lead to enhanced NMDAR signaling is transporter saturation by glutamate pulses arriving at intervals more frequent than the transporter turnover rate. However, glial transporter cycling at 32°C is at least 10-fold faster than the 5-10 Hz frequency threshold for NMDAR signaling (Wadiche and Kavanaugh, 1998; Bergles and Jahr. 1998). Moreover, bursts of up to four stimuli at 100 Hz do not significantly impair glial transport in CA1

(Diamond and Jahr, 2000). However, the effect of pharmacological inhibition shows that during brief repetitive activity, glutamate transport significantly modulates the impact of increasing frequency and release site density on NMDAR signaling (Figure 4.3E).

Consistent with previous work, inhibition of transport during low frequency stimulation leads to enhanced NMDAR activity, as revealed by NMDAR responses in permissive Mg^{2+}-free conditions (Figure 4.1). However, this effect of transport inhibition is not seen in physiological ACSF. Together, these data suggest that during low frequency synaptic transmission, activity of NMDARs is substantially prevented by Mg^{2+} block, and that during repetitive activity, glutamate transport cooperates with Mg^{2+} to limit NMDAR signaling. Modeling of transmitter diffusion in stratum radiatum in the absence of transport suggests glutamate could diffuse and bind to NMDARs associated with hundreds of synapses within 50 ms (Kullmann et al. 1999). In the absence of Mg^{2+}, even with transport intact, glutamate binds to a significant number of NMDARs following a single stimulus, and the time course of the transmitter and receptor occupancy is significantly prolonged by increasing release site density (Figure 4.2B), repetitive activity (Figure 4.1B_1), or transport inhibition (Figure 4.3B).

It is clear from recordings in Mg^{2+}-free conditions that many NMDARs are exposed to synaptic glutamate concentration profiles that are delayed by up to tens of milliseconds relative to AMPAR-mediated fEPSP decay (Figure 4.2B). In physiological conditions, this time delay would tend to limit the voltage-dependent Mg^{2+} unblock of the NMDARs reached by the slow glutamate transient. The time delay is further influenced by release site density (Figure 4.2B) and glutamate transport (Figure 4.7), which would also influence the effective volume of transmitter action.

Together the data indicate that low frequency synaptic activity gives rise to a population of NMDARs that are occupied by glutamate but blocked by Mg^{2+}; these silent NMDARs are primed for activation by subsequent synaptic activity occurring within a time window dependent on the unbinding rate of glutamate from the receptors. Because glutamate unbinding from NMDARs is relatively slow, with a time constant of approximately 200 ms (Lester and Jahr,

1992), activity mediated by such a primed pool of receptors would occur during repetitive activity in excess of ~5 Hz. This rate is in agreement with the measured exponential decay of the inter-stimulus interval we found to activate NMDAR signaling (Figure 4.5, 238ms).. Although voltage-dependent unbinding of Mg^{2+} from glutamate-occupied NMDARs displays complex multi-exponential kinetics, substantial components have time constants in the sub-millisecond range (Kampa et al. 2004), which would allow primed NMDARs activity to essentially follow electrotonic dendritic responses. In addition to frequency, the interaction of release site density and transmitter transport would be expected to influence the size and response of the pool of primed receptors.

NMDAR channel kinetics play a critical role in this priming model, in particular the unbinding rates for glutamate (Lester and Jahr, 1992; Lester et al., 1990) and Mg^{2+} (Mayer et al. 1984; Kampa et al., 2004). Together these rates provide a mechanism for frequency tuning NMDAR responses to repetitive activity near the glutamate unbinding rate, with the onset of activity delayed by one EPSP cycle. This mechanism would be congruent with the minimal requirements of two stimuli for induction of NMDAR-dependent LTP, in which a single synaptic event can prime a postsynaptic neuron such that a subsequent synaptic event within an appropriate time window leads to LTP (Larson and Lynch, 1986). It is notable that 5-10 Hz theta oscillations, which are associated with NMDAR-dependent plasticity in the hippocampus (Buzsaki, 2002), are also near the theoretical threshold frequency determined by transmitter unbinding. This priming mechanism further suggests the possibility that the glutamate affinity and desensitization kinetics of AMPARs could influence the synapse specificity of frequency-dependent NMDAR signaling and LTP induction by favoring Mg unblock in response to the sharper concentration transients coming from closer release sites. Overall, the data indicate that the activity of glutamate transporters is tightly integrated with receptor kinetics to cooperatively control the effects of release site density and frequency on synaptic signaling.

References

Arnth-Jensen N, Jabaudon D, Scanziani M (2002) Cooperation between independent hippocampal synapses is controlled by glutamate uptake. Nat. Neurosci 5:325-331

Asztely F, Erdemli G, Kullmann DM (1997) Extrasynaptic glutamate spillover in the hippocampus: dependence on temperature and the role of active glutamate uptake. Neuron 18:281-293

Attwell D, Gibb A (2005) Neuroenergetics and the kinetic design of excitatory synapses. Nat. Rev. Neurosci 6:841-849

Bergles DE, Jahr CE (1998) Glial contribution to glutamate uptake at Schaffer collateral-commissural synapses in the hippocampus. J Neurosci 18:7709-16

Buzsáki G (2002) Theta oscillations in the hippocampus. Neuron 33:325-340

Christie JM, Jahr CE (2006) Multivesicular release at Schaffer collateral-CA1 hippocampal synapses. J Neurosci 26:210-6

Collingridge GL, Herron CE, Lester RA (1988) Frequency-dependent N-methyl-D-aspartate receptor-mediated synaptic transmission in rat hippocampus. J. Physiol. (Lond.) 399:301-312

Diamond JS, Jahr CE (1997) Transporters buffer synaptically released glutamate on a submillisecond time scale. J Neurosci.17(12):4672-87.

Diamond JS (2005) Deriving the glutamate clearance time course from transporter currents in CA1 hippocampal astrocytes: transmitter uptake gets faster during development. J Neurosci. 25(11):2906-16.

Diamond JS (2001) Neuronal glutamate transporters limit activation of NMDA receptors by neurotransmitter spillover on CA1 pyramidal cells. J. Neurosci 21:8328-8338

Diamond JS, Jahr CE (2000) Synaptically released glutamate does not overwhelm transporters on hippocampal astrocytes during high-frequency stimulation. J Neurophysiol. May;83(5): 2835-43.

Dobrunz LE, Stevens CF (1997) Heterogeneity of release probability, facilitation, and depletion at central synapses. Neuron 18, 995-1008.

Esslinger CS, Agarwal S, Gerdes J, Wilson PA, Davis ES, Awes AN, O'Brien E, Mavencamp T, Koch HP, Poulsen DJ, Rhoderick JF, Chamberlin AR, Kavanaugh MP, Bridges RJ (2005) The substituted aspartate analogue L-beta-threo-benzyl-aspartate preferentially inhibits the neuronal excitatory amino acid transporter EAAT3. Neuropharmacology 49:850-61

Furuta A, Rothstein JD, Martin LJ (1997) Glutamate transporter protein subtypes are expressed differentially during rat CNS development. J. Neurosci 17:8363-8375

Herron CE, Lester RA, Coan EJ, Collingridge GL (1986) Frequency-dependent involvement of NMDA receptors in the hippocampus: a novel synaptic mechanism. Nature 322:265-268

Jabaudon D, Shimamoto K, Yasuda-Kamatani Y, Scanziani M, Gähwiler BH, Gerber U (1999) Inhibition of uptake unmasks rapid extracellular turnover of glutamate of nonvesicular origin. Proc. Natl. Acad. Sci. U.S.A 96:8733-8738

Kampa BM, Clements J, Jonas P, Stuart GJ (2004) Kinetics of Mg2+ unblock of NMDA receptors: implications for spike-timing dependent synaptic plasticity. J. Physiol. (Lond.) 556:337-345

Kullmann DM, Min MY, Asztély F, Rusakov DA (1999) Extracellular glutamate diffusion determines the occupancy of glutamate receptors at CA1 synapses in the hippocampus. Philos. Trans. R. Soc. Lond., B, Biol. Sci 354:395-402

Larson J, Lynch G (1986) Induction of synaptic potentiation in hippocampus by patterned stimulation involves two events. Science 232:985-988

Lester RA, Clements JD, Westbrook GL, Jahr CE (1990) Channel kinetics determine the time course of NMDA receptor-mediated synaptic currents. Nature 346:565-7

Lester RA, Jahr CE (1992) NMDA channel behavior depends on agonist affinity. J Neurosci 12:635-43

Lozovaya NA, Kopanitsa MV, Boychuk YA, Krishtal OA (1999) Enhancement of glutamate release uncovers spillover-mediated transmission by N-methyl-D-aspartate receptors in the rat hippocampus. Neuroscience 91:1321-1330

Mainen ZF, Malinow R, Svoboda K (1999) Synaptic calcium transients in single spines indicate that NMDA receptors are not saturated. Nature 399:151-155

Mayer ML, Westbrook GL, Guthrie PB (1984) Voltage-dependent block by Mg2+ of NMDA responses in spinal cord neurones. Nature 309:261-263

Otis TS, Wu YC, Trussell LO (1996) Delayed clearance of transmitter and the role of glutamate transporters at synapses with multiple release sites. J. Neurosci 16:1634-1644

Rusakov DA, Kullmann DM (1998) Extrasynaptic glutamate diffusion in the hippocampus: ultrastructural constraints, uptake, and receptor activation. J. Neurosci 18:3158-3170

Santos MD, Mohammadi MH, Yang S, Liang CW, Kao JPY, et al. (2012) Dendritic Hold and Read: A Gated Mechanism for Short Term Information Storage and Retrieval. PLoS ONE 7(5): e37542.

Scimemi A, Tian H, Diamond JS (2009) Neuronal transporters regulate glutamate clearance, NMDA receptor activation, and synaptic plasticity in the hippocampus. J. Neurosci 29:14581-14595

Shimamoto K, Lebrun B, Yasuda-Kamatani Y, Sakaitani M, Shigeri Y, Yumoto N, Nakajima T (1998) DL-threo-beta-benzyloxyaspartate, a potent blocker of excitatory amino acid transporters. Mol. Pharmacol 53:195-201

Shimamoto K, Shigeri Y, Yasuda-Kamatani Y, Lebrun B, Yumoto N, Nakajima T (2000) Syntheses of optically pure beta-hydroxyaspartate derivatives as glutamate transporter blockers. Bioorg. Med. Chem. Lett 10:2407-2410

Spruston N, Jonas P, Sakmann B. (1995) Dendritic glutamate receptor channels in rat hippocampal CA3 and CA1 pyramidal neurons. J Physiol. 482

Tong G, Jahr CE (1994) Block of glutamate transporters potentiates postsynaptic excitation. Neuron 13:1195-203

Wadiche JI, Kavanaugh MP (1998) Macroscopic and microscopic properties of a cloned glutamate transporter/chloride channel. J Neurosci 18:7650-61

CHAPTER 5: CONCLUSIONS

In these studies, we investigated glutamate transporter's two important functions in the brain: modulation of ambient glutamate and synaptic glutamate levels. By in vitro expressing glutamate transporters using Xenopus oocyte system, we monitored surface [Glu] as a function of transporter density and confirmed that high density of transporters are capable of maintaining <100nM [Glu] on the surface. With mathematical modeling, we propose that tonic glutamate release in a thin damaged layer near the probe could be a potential cause for the 1000 fold discrepancy of measured ambient glutamate levels between microdialysis and electrophysiological methods. Further, using novel transporter inhibitor L-TBA, we established the specificity and actions of this compound at schaffer collateral synapses in hippocampus and studied the modulation of NMDAR activation by transporters under physiological conditions. We conclude that glutamate transporters, Mg^{2+} and intrinsic kinetics of NMDAR cooperatively determine the frequency activation pattern of NMDAR and potentially its downstream signaling pathways such as long term potentiation. Together, these data demonstrated glutamate transporter's wide concentrational and temporal dynamic range in modulating glutamate signals and its critical roles in maintaining normal brain function. Further studies on the kinetics and structural differences among the 5 EAAT subtypes would further deepen our understanding on the significance of co-expression of different transporter subtypes in the same brain region and transporter's structural roles in capturing glutamate.